

VAPOR + LIQUID EQUILIBRIUM OF WATER, CARBON DIOXIDE, AND
THE BINARY SYSTEM WATER + CARBON DIOXIDE FROM
MOLECULAR SIMULATION

J. Vorholz¹, V. I. Harismiadis², B. Rumpf^{1,3},

A. Z. Panagiotopoulos⁴, G. Maurer^{1,*}

¹ Lehrstuhl für Technische Thermodynamik, Universität Kaiserslautern, D-67653
Kaiserslautern, Germany

² Present address: Hyperion Systems Engineering Ltd., CY-1075 Nicosia, Cyprus

³ Present address: BASF AG, D-67056 Ludwigshafen, Germany

⁴ Institute for Physical Science and Technology and Department of Chemical Engineering,
University of Maryland, College Park, MD 20742, USA

* Author to whom all correspondence should be addressed; e-mail: gmaurer@rhrk.uni-kl.de,
Fax +49 631 205 2410

Keywords: Statistical mechanics, molecular simulation, vapor-liquid equilibria,
enthalpy, density, vapor pressure, mixture, pure components

Abstract

NVT- and NpT-Gibbs Ensemble Monte Carlo Simulations were applied to describe the vapor-liquid equilibrium of water (between 323 and 573 K), carbon dioxide (between 230 and 290 K) and their binary mixtures (between 348 and 393 K). The properties of supercritical carbon dioxide were determined between 310 K and 520 K by NpT-Monte Carlo simulations. Literature data for the effective pair potentials (for water: the SPC-, SPC/E-, and TIP4P-potential models; for carbon dioxide: the EPM2 potential model) were used to describe the properties of the pure substances. The vapor pressures of water and carbon dioxide are calculated. For water, the SPC- and TIP4P-models give superior results for the vapor pressure when compared to the SPC/E-model. The vapor liquid equilibrium of the binary mixture carbon dioxide-water was predicted using the SPC- as well as the TIP4P-model for water and the EPM2-model for carbon dioxide. The interactions between carbon dioxide and water were estimated from the pair potentials of the pure components using common mixing rules without any adjustable binary parameter. Agreement of the predicted data for the compositions of the coexisting phases in vapor-liquid equilibrium and experimental results is observed within the statistical uncertainties of the simulation results in the investigated range of state, i.e. at pressures up to about 20 MPa.

Introduction

The molecular simulation of the thermodynamic properties of fluid mixtures is receiving increasing attention, also due to the rapid development of fast and cheap computers. In molecular simulations, for example Monte Carlo simulations and Molecular Dynamics, the thermodynamic properties of a fluid are determined from information on the pair potential between the encountered molecules. However, as already for small molecules the pair potentials are rarely known, it is state of the art to use „effective“ pair potentials. In expressions for the „effective“ pair potential some more or less adequate approximations are applied to account for e.g. electrostatic or van der Waals interactions between several sites of the molecules in separate contributions. In the literature, a great variety of intermolecular pair potentials for various substances is documented. Especially water has been the subject of numerous examinations (for a review see e.g. [1]), but effective pair potentials are also available for many other polar and non polar substances (an overview over simulation data on the properties of pure liquids and solutions can be found in [2]). The final expression for the „effective“ intermolecular pair potential contains some adjustable parameters which have to be fitted to some experimental data, as e.g. the vapor pressure or the liquid density of the pure component. These optimization procedures require a method to link the pair potential to macroscopic thermodynamic properties. Molecular simulation methods, as e.g. Monte Carlo simulations or Molecular Dynamics simulations offer the possibility to obtain information on the thermodynamic behavior of model fluids interacting with „effective“ pair potentials. In this connection, the simulation of fluid phase equilibria is of particular interest. Techniques like e.g. the NVT- and NpT-Gibbs Ensemble method [3, 4] or alternative implementations such as the NpH-Gibbs Ensemble method [5, 6], the NpT + test particle method [7, 8] or histogram reweighting Monte Carlo methods [9] allow the determination of the phase coexistence curve of fluids from the intermolecular potential.

The aim of the present paper is to test some currently available effective pair potentials for the prediction of the solubility of carbon dioxide in water using molecular simulation. Such a procedure requires at first the choice of appropriate pair potentials for water and carbon dioxide and at second a suitable simulation procedure. In the third step the molecular simulations have to be performed and finally the simulation results have to be compared with experimental data.

Effective intermolecular pair potentials

The quality of the results of a computer simulation on the molecular level depend on the potential model employed to describe the intermolecular interactions between the molecules of the substance studied. So called „effective“ potential models are available for various substances, as e.g. methane and ethane (e.g. [10]), methanol (e.g. [11]), carbon dioxide (e.g. [12] or [13]), ammonia (e.g. [14]), and water (e.g. [15 - 22]).

Rigid fixed-point charge models for water, such as the SPC-model [15], the SPC/E-model [16] or the TIP4P-model [17] are widely used to describe the thermodynamic properties of liquid water at near ambient conditions. The potential parameters of the above-mentioned models are fitted to structural and thermodynamic properties of liquid water at ambient conditions. Therefore, these models are not necessarily suitable for the prediction of phase equilibrium properties particularly at higher temperatures: For example, the TIP4P and the SPC-model were found to yield critical temperatures that are smaller than the experimental values [23, 24], while the SPC/E-model, which is a reparametrization of the SPC-model, gives some improvement regarding the phase coexistence densities [25, 26] as compared to the SPC-model. More highly developed water models are potential models with fluctuating charges or polarizable models (see e.g. [19, 20]). However, no significant improvement

regarding the reproduction of phase coexistence properties was observed in simulations [20, 27].

The SPC, the SPC/E, and the TIP4P potential models were chosen for further investigation, because of their simplicity. In general, a Lennard-Jones potential is used to model the nonpolar interactions, in addition a set of partial point charges is utilized to represent the electron distribution of the molecule. More specifically, in the SPC- and SPC/E-water models, oxygen is modeled as a partially charged Lennard-Jones bead, whereas in TIP4P-water oxygen is represented by a Lennard-Jones site and a partial charge that is moved by the distance r from the oxygen atom towards the hydrogen atoms. In all water models, hydrogen atoms are represented by partial charges without Lennard-Jones contributions. The geometry of the models are shown in Figure 1, the relevant model parameters [15 - 17] are summarized in Table 1.

To enable a combination with the water models, a potential model for carbon dioxide with the same functional form is required. Here, the EPM2-model by Harris and Yung [13] was selected, where the potential parameters were obtained by a scaling procedure to yield good agreement with experimental data for the vapor liquid equilibrium. EPM2-carbon dioxide uses partially charged Lennard-Jones beads for modeling the carbon atom as well as for representing the two oxygen atoms. Its geometry is shown in Figure 2, the potential parameters [13] are given in Table 1.

As all models used in our simulations consist of Lennard-Jones interaction sites and partial point charges in a fixed geometry the total interaction between two molecules i and j with m respectively n interaction sites is calculated as the sum of Lennard-Jones and Coulomb interactions via

$$u_{ij} = \sum_a^m \sum_b^n \left(\frac{1}{4\pi\epsilon_0} \frac{q_i^a q_j^b}{r_{ij}^{ab}} + 4\epsilon_{ij}^{ab} \left[\left(\frac{\sigma_{ij}^{ab}}{r_{ij}^{ab}} \right)^{12} - \left(\frac{\sigma_{ij}^{ab}}{r_{ij}^{ab}} \right)^6 \right] \right), \quad (1)$$

where ϵ_0 is the dielectric constant of the vacuum, q_i^a is the charge on site a of molecule i, r_{ij}^{ab} is the distance between sites a and b, and σ_{ij}^{ab} and ϵ_{ij}^{ab} are Lennard-Jones interaction parameters between sites a and b located at molecules i and j.

For the Lennard-Jones interactions between unlike atoms the Lorentz-Berthelot combining rules were used. The cross interactions between the unlike Lennard-Jones sites of the carbon dioxide molecules were calculated using the geometric mean for both, core diameter and energy well depth [13], whereas the Lennard-Jones interactions were calculated using the arithmetic mean of the core diameters and the geometric mean of the well depths in any other case:

$$\begin{aligned}\sigma_{ij}^{ab} &= \sqrt{\sigma_i^a \sigma_j^b} \quad \text{for } a,b = \text{C}_{\text{CO}_2}, \text{O}_{\text{CO}_2} \\ \sigma_{ij}^{ab} &= \frac{1}{2}(\sigma_i^a + \sigma_j^b) \quad \text{elsewhere}\end{aligned}\tag{2}$$

$$\epsilon_{ij}^{ab} = \sqrt{\epsilon_i^a \epsilon_j^b}\tag{3}$$

Simulation method

Monte Carlo (MC) simulations usually employ several hundreds of particles within periodic boundary conditions (c.f. [28]). Starting from an arbitrary initial configuration a very large number of configurations (typically $O(10^6 - 10^7)$) is generated according to certain rules. Before information is collected for thermodynamic property calculation during the so called „production“ period, the system is given the opportunity to evolve towards equilibrium in a sufficiently large (usually several millions of configurations) „equilibration“ period. Equilibrium is reached when the observed thermodynamic properties of the system fluctuate around constant values.

In the present work, the following simulation procedures were utilized: The Gibbs Ensemble Monte Carlo technique (GEMC) is particularly suited for the direct simulation of phase equilibria. Therefore, the canonical version (NVT-GEMC) was applied here to determine the saturation properties of the pure fluids water and carbon dioxide and the isothermal-isobaric version (NpT-GEMC) for calculating the vapor-liquid equilibrium of the binary system carbon dioxide + water. Conventional Monte Carlo simulations in the isothermal-isobaric ensemble (NpT-MC) were applied for calculating thermodynamic properties of carbon dioxide in the single phase region. The NpT-MC simulations followed the common procedure which has been described in detail (c.f. [28]), thus no details are repeated here. A detailed description of the Gibbs Ensemble method is also available in the literature (c.f. [3, 4]). Nevertheless it is worthwhile to present some features of this method here:

In the NVT- as well as in the NpT-version of the Gibbs Ensemble technique two phases at equilibrium are simulated at a fixed number of molecules and a given temperature. For this, a Monte Carlo simulation is set up in the instable or metastable region of a system, that is divided into two subsystems. In the course of the simulation, the system forms two homogeneous phases in the separate subsystems, which are designated in the following by superscripts I (liquid) and II (vapor). The phase separation is achieved by three types of Monte Carlo moves, which include changes in the position and orientation of arbitrarily selected molecules in a phase (to ensure equilibration within each region), exchanges of particles between the coexisting phases (to equilibrate the chemical potentials of each component) and volume changes of both phases (to ensure the equality of the pressure in both phases). In an NVT-GEMC simulation the decrease of the volume of one phase is compensated by an increase of equal size of the volume of the other phase, as the total volume of the system - i.e. the sum of the volumes of both phases - has to be kept constant. In an NpT-GEMC simulation the coexistence pressure instead of the total volume is specified and so there is no similar

restriction for the volume changes of the coexisting phases. A move is accepted or discarded when it fulfills or contradicts certain so called „acceptance criteria“ (c.f. appendix).

Often, the transfer move is a bottleneck in achieving convergence in GEMC simulations at high number densities. In dense fluids it becomes difficult to find energetically favorable spots (i.e. „holes“) in the fluid to successfully insert a particle. As a consequence almost all attempted transfers are rejected. Several techniques to enhance the efficiency of the transfer step have been proposed in the literature, e.g. „orientational biasing“ for molecules with a strongly orientation dependent potential [29] or „configurational biasing“ for long chain molecules [30]. In the present work, an alternative procedure is applied. This method is a modification of the procedure developed by Loyens et al. [31] for GEMC simulations on parallel computers and utilizes trial particle insertions. Details on the moves and acceptance criteria used in the present work are described in the appendix.

For completeness, it should be added, that the Gibbs Ensemble technique cannot be applied in the vicinity of critical points as vapor-liquid coexistence can no longer be observed because of finite size effects [32].

In general, the acceptance criteria require the knowledge of the system energy. In the present work, the Lennard-Jones part of the intermolecular energy was calculated with a method proposed by Theodorou and Suter [33], the contribution of the Coulomb interactions was estimated via Ewald sums (ES) [34] in vacuum boundary conditions.

The residual energy, the density, and the concentration were obtained by ensemble averaging in the production period:

$$\delta u = \left\langle \sum_{i<j} u_{ij} \right\rangle \quad (4)$$

$$\rho = \left\langle \frac{\sum_j N_j M_j}{N_A V} \right\rangle \quad (5)$$

$$x_i = \left\langle \frac{N_i}{\sum_j N_j} \right\rangle \quad (6)$$

The angular brackets denote the ensemble average. u_{ij} denotes the intermolecular interactions between molecules i and j . δu , N_i , and V stand for energy, the number of molecules of component i and the volume in the respective phase, M_i is the molecular weight of component i , and N_A is Avogadro's number. The pressure p was determined during NVT-GEMC simulations by a method where the volume fluctuations ΔV of the Gibbs Ensemble can be used to evaluate the pressure of the system at almost zero computational cost [35]. Here, the following ensemble average is calculated during the production period for each phase:

$$p(\Delta V) = \frac{kT}{\Delta V} \ln \left\langle \left(\frac{V + \Delta V}{V} \right)^N \exp \left(-\frac{\Delta u}{kT} \right) \right\rangle \quad (7)$$

In the above equation, V and N represent the volume and the number of molecules of the phase for which the pressure is evaluated. ΔV stands for a volume change leading to the energy difference Δu in the respective phase, T is the temperature and k denotes Boltzmann's constant. During production the value of the volume change has to be kept constant in order to evaluate the pressure of the system correctly. Equation (7) yields two pressure values per phase, one due to positive volume changes (ΔV^+), and one due to negative volume changes (ΔV^-). The final value for the pressure was taken as the arithmetic mean of both values.

Usually, the pressure results calculated from the change of the internal energy of the liquid phase are subjected to large fluctuations. Hence, in most cases reported pressures were calculated from volume changes of the gas phase as described above.

The residual part of the enthalpy of a pure component is calculated from the sum of the residual part of the internal energy and the pressure

$$\delta h = \delta u + \frac{p}{\rho} - RT, \quad (8)$$

where R denotes the individual gas constant of the component. In the case of NVT-GEMC simulations the ensemble average of the pressure was used in the above equation, whereas it was set to the specified pressure during the simulations with $(N, p, T) = \text{const.}$

The heat of vaporization Δh^v of a pure component equals the difference between the residual part of the enthalpies in the vapor and the liquid phases:

$$\Delta h^v = (\delta u^{\text{II}} - \delta u^{\text{I}}) + p \left(\frac{1}{\rho^{\text{II}}} - \frac{1}{\rho^{\text{I}}} \right). \quad (9)$$

This equation is only correct when the contributions from the translational, rotational and vibrational degrees of freedom of the molecules do not differ in the coexisting phases.

In general, averaging was not started before the fluctuations of all of the properties of interest, i.e. densities, energies, volumes, pressure (in the case of NVT-GEMC simulations) and concentrations of the different species (in the case of the simulations of the vapor - liquid equilibrium of the binary mixture) indicated that equilibrium was reached. The statistical uncertainties of the simulation results were estimated by dividing the whole production period into 5 to 15 (depending on the length of that period) blocks of equal size and calculating the standard deviation of the block averages of the thermodynamic properties.

Simulation details, results, and discussion

Comparison of the results for pure components water and carbon dioxide; Test of simulation software

The developed simulation code was checked by comparing the simulation results with literature simulation data for the vapor-liquid equilibrium of the pure components water and carbon dioxide. As the simulation of the vapor - liquid equilibrium of water and carbon dioxide employing the SPC-, the SPC/E-, the TIP4P- and the EPM2-model was already subject of former studies (c.f. [13, 21 - 26, 29, 36]) only a graphical presentation of the VLE - results is given (Figure 3 - Figure 13, the according tables are available, c.f. section „Supplementary material“). The literature data used for comparison (see Table 2) are based on the same potential models, however, in some cases different simulation methods and different techniques for the treatment of the system energies and the pressure calculation were employed. Furthermore, biasing methods were applied by some authors. The Bender equation of state [37] is used for the comparison with experimental data of the pure components. In the following we refer to these results also as „experimental data“.

Simulation details and results for water

Simulation details

The system size varied between 140 and 350 molecules. The runs included between 5 and 20 millions of configurations, the equilibration period typically required about 1 to 5 millions of configurations. The length of a run was influenced by the number of molecules, the state point investigated and depended also on how far from equilibrium the simulation was started.

Depending on the system temperature about 1 to 50 trial insertions per transfer move were performed in the simulations with the SPC- and the TIP4P-model, whereas that number was increased up to 70 when the SPC/E-model was applied at low temperatures. The low

acceptance rate for molecule transfers to the liquid phase was one of the main difficulties in the simulations. Despite multiple trial insertions that acceptance ratio was less than or equal 0.1% (for the SPC/E-model) and 0.6% (for the SPC- and the TIP4P-model) at temperatures below 423.15 K. Consequently, the number of transfers went down to the order of 10^3 - 10^4 successful exchanges per run at the lowest temperature (323.15 K) when the SPC- and the SPC/E-model was used, while it was still around 10^5 for the TIP4P-model. At higher temperatures the numbers of transfers were of the order of 10^5 - 10^6 successful exchanges per run.

Another problem arose from the low density of the saturated vapor phase especially at lower temperatures. Despite its comparatively large volume the vapor phase was alternately empty or populated by only very few molecules over long periods of the simulation (see also [38]) leading to larger fluctuations in the gas phase properties. In the present work, during production the average particle number in the gas phase was between 1 and about 10 in the TIP4P-runs at temperatures up to 423.15 K, and for the SPC- and the SPC/E-models at temperatures up to 473.15 K. The maximum average particle number in the gas phase was around 40 for SPC-water, 30 for SPC/E-water and 80 for TIP4P-water at the highest temperature.

During the production period of the simulations employing the SPC-model the (constant) volume change for the calculation of the saturation pressure (cf. equation 7) varied between 0.8% and 1.7% of the volume of the accompanying liquid phase resulting in acceptance ratios for the volume change (cf. appendix) between 40% and 70%. In the simulations with the SPC/E- and the TIP4P-model that relative volume change varied from 0.6% to 1.2% and from 1.0% to 1.7%, respectively. The resulting acceptance ratios varied between 45% and 67% (SPC/E) and from 38% to 64% (TIP4P).

During the production period of the simulations the (constant) volume change for the calculation of the saturation pressure (cf. equation 7) typically varied between 1% and 2% of the volume of the accompanying liquid phase resulting in acceptance ratios for the volume change (cf. appendix) between 40% and 70%.

The obtained acceptance ratios for the particle translations and rotations within the liquid phase were between 35% and 45%, and between 35% and 90% (in some cases up to 100%) in the vapor phase.

In both phases, the total intermolecular energy mainly resulted from the long-range Coulomb interactions. In the liquid phase the magnitudes of the Coulomb energies were typically of the order of 6 - 9 times the respective Lennard-Jones contribution, in the gas phase between 5 and up to 14 times.

Results

Figures 3 to 5 show the influence of the temperature on the density of the coexisting phases. It can be seen that the results of the present work agree well with literature simulation data. The statistical uncertainties of the simulation results of the present work for the liquid densities are typically between 1% and 7% in the case of SPC- and SPC/E-water, and between 1% and 5% for TIP4P-water, with the maximum values at the highest temperature. For the gas phase densities the statistical uncertainty varies from 5% to 20%, 5% to 35%, and 5% to 95% in the simulations with the TIP4P-, SPC-, and the SPC/E-model, respectively. Here the maximum uncertainties occur at the lower temperatures mainly due to the very small number for the density.

For the liquid phase density the agreement between simulation and experiment is best for the SPC/E-model, followed by the TIP4P- and the SPC-model. For the vapor phase density the agreement between 323.15 K and 523.15 K is best in the case of SPC-water, while the SPC/E-

and the TIP4P-models predict densities that deviate between 40% and 60% from the experimental values. Above 523.15 K all models yield strong deviations from experiment.

In the case of SPC-water the differences between the computed and experimental densities of the saturated vapor between 323.15 K and 473.15 K are generally lower than 20% and within the statistical uncertainty of the simulation results. At higher temperatures, the gas phase density is overestimated (up to about 160% at 553.15 K). The predictions of the SPC-model for the liquid phase densities are too small (between 3% at 323.15 K and 30% at 553.15 K). When the SPC/E-model is used, the liquid densities are also underestimated (by about 2% at 373.15 K and by about 13% at 573.15 K). Furthermore, the predictions for the gas phase density are too small (deviations between 35% and 60%). The TIP4P-model gives predictions for the vapor phase density which are too large (between about 40% and 60% below 523.15 K, and up to about 130% above), whereas the liquid density is underestimated (between 2% at 323.15 K and up to 47% at 573.15 K).

Figure 6 shows a comparison of the new simulation results for the saturation pressure with literature simulation data from [21] as well as with experimental results. In the present work, the statistical uncertainty for the vapor pressure is between 7% and 70% in the simulations with SPC-water, between 5% and 65% in the case of SPC/E-water, and between 5% and 17% in the TIP4P-water simulations. Again, the maximum uncertainty occurs at low temperatures and small densities, respectively.

In view of the usually large fluctuations occurring in pressure calculations the agreement between the vapor pressures calculated by equation (7) and by the method applied by Boulougouris et al. (virial function) is good. It can be seen that the SPC-model yields vapor pressures in better agreement with experimental data than the two other potential models.

The enthalpy of vaporization as calculated from the different water models are plotted in Figure 7. The SPC/E-model systematically overestimates the experimental value over the

whole simulated temperature range. The agreement between the SPC- and TIP4P-model and experiment is better below 373.15 K, at higher temperatures large and systematic deviations are observed for both models. A comprehensive presentation of the results is given in a p - δh -diagram (Figure 8).

Repeated simulations employing different simulation parameters were carried out for SPC-water at 423.15 K, 473.15 K, and 523.15 K and for SPC/E-water at 573.15 K. An influence of the system size on the results was observed only once in the case of SPC-water at 423.15 K. Here, a larger average number of molecules in the gas phase (3 as compared to one) led to a slightly enhanced vapor density that caused a higher vapor phase energy. However, the quantitative study of this system size effect is not the subject of this paper. For a detailed discussion of possible consequences of the fact that very different particle numbers may appear in the two cells of an NVT-GEMC simulation the reader is referred to [39]. In the present work, repeated simulations with the SPC- and the SPC/E-model revealed no significant influence of the magnitude of the volume change on the results for the saturation pressure. Finally, the good agreement with the simulation data from the literature for the densities of the saturated vapor and the vapor pressure prove that the system size and the particle distribution over the two subsystems have only a minor influence on the results. The results from the comparisons with experimental data resulted in selecting the SPC-model as first and the TIP4P-model as second choice for the water pair potential for the further investigation of the thermodynamic properties of the binary mixture carbon dioxide + water.

Simulation details and results for carbon dioxide

Simulation details

The system size varied between 250 and 350 molecules in the NVT-GEMC simulations, 50 and 250 particles were employed in the NpT-MC simulations. The NVT-GEMC runs consisted of 6 to 12, in one case of 18 millions of configurations. In most cases the NpT-MC simulations included between 1 and 5 million configurations and needed less than 0.5 millions of configurations to equilibrate. Close above the critical point of carbon dioxide (at $T \approx 310 \text{ K} - 320 \text{ K}$, $p \approx 10 \text{ MPa}$), the density and enthalpy undergo a rapid change with increasing pressure. Here, the 250 particle systems needed up to 4.5 millions of configurations to equilibrate, the total length of the simulation was extended to up to 17 millions of configurations. For the 50 particle systems it took only around 1 million configurations to equilibrate, the simulation included a total of 3.6 millions of configurations.

Due to the lower number density of liquid carbon dioxide (as compared to water at the same temperature) one to 5 trial insertions per attempted transfer, respectively, were found to be sufficient in the NVT-GEMC runs. The corresponding transfer acceptance ratios were between 0.4% and 3%. The effect that very small numbers of particles appeared in the gas phase was less pronounced in the EPM2 runs than in the runs employing the water models. In all runs on average at least 10 molecules were present in the gas phase during production, the maximum number was around 60 at 290.15 K. The (constant) volume change varied between 1% and 2% of the volume of the respective liquid phase resulting in acceptance ratios between 35% and 60%. The acceptance ratios for the particle displacements were about the same as for water, i.e. between 30% and 50% in the liquid phase, and between 40% to 90% in the gas phase.

NpT-MC simulations only employ particle displacements and volume changes. The obtained acceptance ratios for the displacements were between 40% at high densities and 96% at low densities and between 50% and 75% for the respective volume changes.

In contrary to the water simulations, the total system energy was dominated by the Lennard-Jones interactions. In the liquid and the vapor phase the ratio of the magnitudes of Lennard-Jones to Coulomb energies was typically between 4 and 5, and increased to values between 7 to 25 in the supercritical region at 520 K.

Results

The comparison between simulation results and experimental data for the vapor-liquid equilibrium of carbon dioxide is shown in Figures 9 to 13. The simulation results of the present work are consistent with the simulation results of Harris and Yung [13].

Figure 9 shows the densities of the coexisting phases. The differences between the simulation results and experimental data are smaller than about 3% and 16% for the density of the liquid and the vapor phase, respectively. In most cases the differences are within the statistical uncertainties of the results of the present work (liquid density: 0.5% - 4%; vapor density: 5% - 15%). Figure 10 shows the comparison between simulation and experiment for the vapor pressure. The EPM2-model slightly overestimates the vapor pressure of carbon dioxide, however the deviations are always smaller than 15% and in most cases within the statistical uncertainties of the simulation results which are typically between 3% and 8% in most cases and increase to 20% at lower temperatures. The experimental values for the heat of vaporization could be reproduced within the statistical uncertainties over the whole simulated temperature range with the exception of one point at 290.15 K (Figure 11) which deviates from the experimental value by about 4%.

The behavior of the model in the supercritical region was of particular interest as the simulations for the binary mixture carbon dioxide-water were carried out at temperatures and pressures above the critical properties of carbon dioxide. Therefore, the thermodynamic properties of EPM2-carbon dioxide were compared with experimental data at 310.0 K, 320.0 K, 350.0 K, 390.0 K, and 520.0 K. The results are summarized in Figure 12 (pressure versus density) and Figure 13 (pressure versus residual enthalpy). A numerical comparison is also available (c.f. section „Supplementary material“). Typically, the statistical uncertainties of the simulation results are below 3%, with the exception of the simulations that were carried out close, but above the critical point. Here the maximum uncertainty reaches around 20%. Although the differences between the results of the simulation and experiment are sometimes and particularly for the enthalpy beyond the statistical uncertainties of the simulation results, the agreement is encouraging.

Simulation details and results for the binary system carbon dioxide-water

Simulation details

NpT-GEMC simulations were carried out with two different model combinations. The EPM2-model for carbon dioxide was combined with the SPC- as well as with the TIP4P-model for water, respectively. The simulations employed 300, 450, and 600 molecules. In all simulations the overall ratio of water molecules to carbon dioxide molecules was 2:1. The simulations were either started from the two cells containing the pure components with densities sufficiently far away from the expected equilibrium densities or from output configurations of former runs. Depending on the system size, the state point investigated, and the starting point of the simulation, the runs included between 8 and 33 millions of configurations. Most of the simulations were equilibrated after a few million configurations, in some cases it took up to 11 million configurations for the system to reach equilibrium.

Between (25 and 70), and (25 and 40) trial insertions per attempted transfer move were employed for each species in the simulations when combining EPM2-carbon dioxide with SPC- and TIP4P-water, respectively. In general, it was more difficult to achieve successful transfers for water than for carbon dioxide. Depending on temperature and pressure the finally obtained transfer acceptance ratios varied between 0.2% and 1% for water and from 0.6% to 3% for carbon dioxide. Altogether, between 10^5 - 10^6 successful transfers per species and run were achieved. It should be noted that - as a consequence of the relatively small solubility of carbon dioxide in water - only few (< 10) carbon dioxide molecules were present in the liquid phase. In the gas phase average numbers of water molecules between one (at 348.15 K and high pressures) and around 30-40 (at 393.15 K and low pressures) were observed.

The finally achieved volume acceptance ratios ranged from 30% to 70% in the liquid phase and from 50% to 80% in the vapor phase. The obtained acceptance ratios for the particle displacements in the liquid phase were typically around 30% - 50% for water and 30% - 80% for carbon dioxide. Between 40% and 90% successful particle displacements were achieved in the gas phase for both species.

In general, repeated independent simulations with different acceptance ratios for the respective moves revealed no significant influence on the simulation results.

As expected from the simulations of the pure fluids the interactions in the (water rich) liquid phase were dominated by the Coulomb contribution in contrast to the vapor phase (mainly consisting of carbon dioxide). In the liquid phase the magnitude of the electrostatic contributions typically equaled 7-8 times the Lennard-Jones part, whereas the Lennard-Jones interactions equaled up to 6 times the Coulomb energy in the gas phase.

Results

NpT-GEMC simulations of the binary system carbon dioxide + water were carried out at 348.15 K, 373.15 K, and 393.15 K. The results are summarized in Figures 14-19 and Tables 3 and 4.

The statistical uncertainties for the concentrations of water in the gas phase range from about 5% to about 30% at 373.15 K and 393.15 K, and from about 8% to 40% at 348.15 K. The uncertainties for the gas phase concentration of carbon dioxide are lower than 1% at 348.15 K and 373.15 K and lower than 2% at 393.15 K. In the liquid phase the statistical uncertainties of the results for the molality of carbon dioxide vary in most cases between 10% and 40% for the runs with the SPC-model, and between 13% and 26% for the runs with the TIP4P-model for water. The statistical uncertainties of the simulation results for the densities are in most cases smaller than 1% for the liquid, and between 1% and 6% for the gas phase.

The simulation results for the equilibrium concentrations of the coexisting phases are compared with experimental data [40 - 46] and a correlation for the solubility of carbon dioxide in water [47].

The comparison for the system SPC-water + EPM2-carbon dioxide is shown in Figures 14-16. The results of repeated independent simulation runs reveal some scattering especially in the liquid phase, however, they agree within their statistical uncertainties. The simulation correctly predicts that the solubility of water in the vapor phase increases with temperature, whereas the solubility of carbon dioxide in the liquid phase does not change significantly within the investigated temperature range.

Figure 17 shows the densities of the coexisting phases in the binary system EPM2-carbon dioxide + SPC-water at 393.15 K in comparison with results from the Bender equation of state for the densities of the pure components [37], predictions by the generalized Bender equation for the binary system [48] and experimental data for the liquid density [46].

As the concentration of water in the gas phase is small, the density of the gas phase is approximately the same as the vapor density of pure carbon dioxide. But as the EPM2 model yields good estimates for the experimental density of pure carbon dioxide also in the supercritical region, the agreement between the simulation results and the experimental data is good. Deviations are within the statistical uncertainty of the simulation results. The liquid phase mainly consists of water. The liquid density of the binary mixture is underestimated because the SPC-model underestimates the liquid density of pure water. The generalized Bender equation [48] predicts an increase in the liquid density with increasing pressure and carbon dioxide concentration, however, the experimental data of Nighswander et al. [46] show densities that are slightly smaller than the density of pure water. Similar results for the densities were obtained at 348.15 K and 373.15 K.

For comparison, the phase behavior of the system EPM2-carbon dioxide + TIP4P-water at 393.15 K is shown in Figures 18 and 19. Besides a slightly smaller solubility of water in carbon dioxide in the gas phase no significant changes in the equilibrium concentrations are observed. However, the predicted density of the liquid phase is higher as the TIP4P-model was found to yield liquid densities that are closer to experimental data than the predictions from the SPC-model. Similar behavior was observed at 348.15 K (see section „Supplementary material“).

Conclusions

Molecular simulation techniques enable the calculation of thermodynamic properties of fluid systems from information on interactions on the molecular level. However, before these methods can be introduced into engineering business extensive tests on - at least and at first - simple model systems are required.

The present contribution aims to predict the phase equilibrium of the binary system carbon dioxide-water by molecular simulation and to compare the results with experimental data. As the main interest is on predictions, the intermolecular pair potential for interactions between water and carbon dioxide was estimated from the effective pair potentials of the pure components by applying commonly used mixing rules without any binary interaction parameters. As differences between simulation results and experimental data for the mixture might be - at least in some parts - caused by approximations already introduced in the models for the pure components, the thermodynamic properties (mainly the saturation properties) of the pure components water and carbon dioxide are also calculated and discussed. Simulation results for the vapor liquid equilibrium of the binary system carbon dioxide-water favorably agree with experimental data. Although the differences are still larger than the experimental uncertainties for most properties, the good agreement encourages one to study such methods also for predicting the thermodynamic properties of other and also of more complicated aqueous mixtures.

Supplementary material

Tables containing the simulations results for the vapor liquid equilibrium of water using the SPC-, SPC/E-, and TIP4P-model, and for carbon dioxide employing the EPM2-model, as well as additional data on the vapor liquid equilibrium in the system EPM2 - carbon dioxide + TIP4P - water are available. Ordering information is given on any current masthead page.

Acknowledgments

This work was started when JV, VIH, and AZP were at the School of Chemical Engineering at Cornell University, Ithaca, USA.

Supercomputing time was provided by the Regionales Hochschulrechenzentrum Kaiserslautern (RHRK) and the Cornell Theory Center (CTC). JV gratefully acknowledges a scholarship of the Deutscher Akademischer Austauschdienst (DAAD). VIH would like to thank Shell Research Technical Center, Amsterdam for some support.

List of Symbols

Latin

B	pseudo Boltzmann factor
C	carbon
h	enthalpy
k	Boltzmann's constant
N	number of molecules
M	molecular weight
n_{trial}	number of trials
N_A	Avogadro's number
O	oxygen
P	probability
p	pressure
q	charge
R	Gas constant
r	distance
T	temperature
u	energy
V	volume
x	mole fraction
y	mole fraction
Z	Rosenbluth weight

Greek

α	bond angle, parameter in acceptance criterion
Δ	change
δ	residual
ε	Lennard-Jones well depth
ε_0	dielectric constant
π	pi
ρ	density
σ	Lennard-Jones diameter
ξ	random number

Subscripts

C	carbon
CO ₂	carbon dioxide
H	hydrogen
i	position, atom, molecule, component
j	atom, molecule, component
k	trial
M	charge position
mod	modified
O	oxygen
0	original position

Superscripts

a	site
b	site
LJ	Lennard-Jones
(new)	new configuration
(old)	old configuration
V	vaporization
I	liquid phase
II	vapor phase
+	positive
-	negative

Appendix

Acceptance criteria and simulation parameters

In Monte Carlo simulations the criteria for the acceptance of a certain move are usually derived considering the partition function of the ensemble of interest taking into account the condition of „microscopic reversibility“ (c.f. e.g. [28]). Although the acceptance criteria for the Gibbs Ensemble can be found in the literature (e.g. [3, 4]), they are summarized here once more for convenience:

In GEMC simulations three different moves (molecule displacements, molecule transfers, and volume changes of the two subsystems) are employed. For each move a so called “pseudo Boltzmann factor” B is considered:

$$B = \alpha \exp \left[- \frac{(\mathbf{u}^{(\text{new})} - \mathbf{u}^{(\text{old})})}{kT} \right] \quad (10)$$

u denotes the residual part of the internal energy of a configuration before (old) and after (new) a move. The parameter α depends on the type of move:

a) molecule displacement $\alpha = 1$ (10 a)

b) molecule transfer (e.g. from phase II to phase I): $\alpha = \frac{(N^{\text{II}} + 1)V^{\text{I}}}{N^{\text{I}}V^{\text{II}}}$ (10 b)

c) volume change ΔV : $\alpha = \left(\frac{V^{\text{I}} + \Delta V^{\text{I}}}{V^{\text{I}}} \right)^{N^{\text{I}}} \left(\frac{V^{\text{II}} + \Delta V^{\text{II}}}{V^{\text{II}}} \right)^{N^{\text{II}}}$ (10 c)

A move with $B > 1$ is always accepted. In any other case a random number ξ is generated uniformly on the interval $[0,1]$ and compared with B . The move is accepted if $\xi \leq B$, otherwise it is discarded (c.f. [28]). This procedure ensures that each configuration is created with its proper statistical weight.

The molecule transfer from the vapor phase to the liquid phase can cause problems at high densities as it might be difficult to find an empty „space“ in the liquid phase. In order to achieve a reasonable number of successful molecule transfers, the transfer procedure and acceptance criterion for the transfer move were modified based on a technique originally proposed by Loyens et al. [31]:

The modified procedure starts from the assumption that at short distances the repulsive part of the Lennard-Jones contribution dominates the intermolecular interactions. That means that at high densities the energetically favorable „holes“ can be located by considering only the Lennard-Jones part of the intermolecular potential, i.e. in particular, that the computationally expensive calculation of the long-range Coulomb contributions can be avoided. The molecule to be transferred to (e.g. from phase I to phase II) was picked randomly and the Lennard-Jones energy of its position was calculated. After that n trial positions were picked randomly in phase II and the Lennard-Jones energy of each position $u_k^{\text{LJ}(\text{new})}$, where $k \in [1, \dots, n]$, and the according Rosenbluth weight $Z^{\text{LJ}(\text{new})}$ was computed:

$$Z^{\text{LJ}(\text{new})} = \sum_{k=1}^n \exp\left[-\frac{u_k^{\text{LJ}(\text{new})}}{kT}\right]. \quad (11)$$

One trial position, e.g. the i^{th} , was then picked with probability

$$P_i^{(\text{new})} = \frac{\exp\left[-\frac{u_i^{\text{LJ}(\text{new})}}{kT}\right]}{Z^{\text{LJ}(\text{new})}} \quad (12)$$

This was realized by creating a random number ξ uniformly on the interval [0,1] and selecting

the position i for which the condition $\sum_{k=1}^{i-1} P_k < \xi \leq \sum_{k=1}^i P_k$ was fulfilled. This procedure favors a

position with a low energy, but it introduces a bias which violates the principle of

„microscopic reversibility“. The bias is removed in the final acceptance criterion by modifying equation (10) in analogy to the method of Loyens et al. [31]:

$$B_{\text{mod}} = \alpha \exp \left[-\frac{(u^{(\text{new})} - u^{(\text{old})})}{kT} \right] \frac{\exp \left[-\frac{u_0^{\text{LJ}(\text{old})}}{kT} \right] Z^{\text{LJ}(\text{new})}}{\exp \left[-\frac{u_i^{\text{LJ}(\text{new})}}{kT} \right] Z^{\text{LJ}(\text{old})}} \quad (13)$$

In this equation $u_0^{\text{LJ}(\text{old})}$ denotes the Lennard-Jones energy of the original position of the molecule to be transferred in phase I, $u_i^{\text{LJ}(\text{new})}$ is the Lennard-Jones energy of the pre-selected trial position in phase II (c.f. equation (11)), $u^{(\text{old})}$ and $u^{(\text{new})}$ stand for the total energy of the system before (old) and after (new) the transfer of the molecule from the old to the pre-selected position, and $Z^{\text{LJ}(\text{new})}$ follows from equation (11). $Z^{\text{LJ}(\text{old})}$ is calculated in a similar way:

$$Z^{\text{LJ}(\text{old})} = \exp \left[-\frac{u_0^{\text{LJ}(\text{old})}}{kT} \right] + \sum_{k=1}^{n_{\text{trial}}-1} \exp \left[-\frac{u_k^{\text{LJ}(\text{old})}}{kT} \right], \quad (14)$$

but now $u_k^{\text{LJ}(\text{old})}$ is the Lennard-Jones contribution to the energy of a virtual molecule at a randomly chosen position in phase I. The final acceptance procedure follows the method described above (i.e. select a random number $\xi \dots$ etc.).

During Monte Carlo simulations the order of the moves to be performed is usually selected at random, but each move occurs with a certain frequency in order to ensure equilibration and stability of the simulation. In the NVT-GEMC simulations of the present work the ratio of attempted moves was typically between 25% - 94% particle displacements, 1% - 2% volume fluctuations and 6% - 75% particle transfers, in the NpT-GEMC simulations it was 40% and 50% for the particle displacements, 1% volume changes and 50% and 60% particle transfers. The NpT-MC simulations normally employed 96% or 98% particle displacements and 2% or

4% volume fluctuations, one simulation was carried out with 80% particle displacements and 20% volume fluctuations.

The ratio of accepted to attempted moves (i.e. the acceptance ratio) depends on the magnitude of the changes performed. The maximum changes in position and orientation of a molecule were adjusted to obtain a 40% - 50% acceptance rate for the attempted move, where possible. The maximum allowed volume change was set to 3% of the volume of the respective phase in both, NpT-MC and NpT-GEMC simulations, while it was limited to 3% of the liquid phase volume in NVT-GEMC simulations.

In the case of the binary system, the number of attempted transfers per species was adjusted during the simulation in a way that approximately the same number of successful transfers was achieved for each species [4].

Literature

- [1] S. B. Zhu, S. Singh, G. W. Robinson, Field perturbed water, *Chem. Phys. Ser.* 85 (1994) 627
- [2] Y. M. Kessler, Y. P. Puhovski, M. G. Kiselev, I. I. Vaisman, Computer Simulations of Liquid Systems: Possibilities and Principal Results, in *Chemistry of Nonaqueous Solutions: Current Progress*, G. Mamantov, A. I. Popov (Eds.), Wiley, Chichester (1994) 307
- [3] A. Z. Panagiotopoulos, Direct Determination of Phase Coexistence Properties of Fluids by Monte Carlo Simulation in a New Ensemble, *Mol. Phys.* 61 (1987) 813
- [4] A. Z. Panagiotopoulos, N. Quirke, M. Stapleton, D. J. Tildesley, Phase Equilibria by Simulation in the Gibbs Ensemble: Alternative Derivation, Generalization and Application to Mixture and Membrane Equilibria, *Mol. Phys.* 63 (1988) 527
- [5] T. Kristóf, J. Liszi, Alternative Implementations of the Gibbs Ensemble Monte Carlo Calculation, *Chem. Phys. Lett.* 261 (1996) 620
- [6] T. Kristóf, J. Liszi, Alternative Gibbs Ensemble Monte Carlo implementations: Application in Mixtures, *Mol. Phys.* 94 (1998) 519
- [7] D. Möller, J. Fischer, Vapour-liquid Equilibrium of a Pure Fluid from Test Particle Method in Combination with NpT Molecular Dynamics Simulations, *Mol. Phys.* 69 (1990) 463
- [8] A. Lotfi, J. Vrabec, J. Fischer, Vapour Liquid Equilibria of the Lennard-Jones Fluid from the NpT plus Test Particle Method, *Mol. Phys.* 76 (1992) 1319
- [9] A. M. Ferrenberg, R. H. Swendsen, New Monte Carlo Technique for Studying Phase Transitions, *Phys. Rev. Lett.* 61 (1988) 2635
- [10] A. Lotfi, Molekulardynamische Simulationen an Fluiden: Phasengleichgewicht und Verdampfung, PhD-thesis, Ruhr-Universität Bochum, Germany, see also Fortschrittsberichte VDI, Reihe 3, Nr 335 (VDI-Verlag Düsseldorf, 1993)
- [11] M. van Leeuwen, B. Smit, Molecular Simulation of the Vapor-Liquid coexistence Curve of Methanol, *L. Phys. Chem.* 99 (1995) 1831
- [12] D. Möller, J. Fischer, Determination of an Effective Intermolecular Potential for Carbon Dioxide Using Vapour-Liquid Phase Equilibria from NpT + test particle simulations, *Fluid Phase Eq.* 100 (1994) 35
- [13] J. G. Harris, K. H. Yung, Carbon Dioxide's Liquid-Vapor Coexistence Curve and Critical Properties As Predicted by a Simple Molecular Model, *J. Phys. Chem.* 99 (1995) 12021
- [14] T. Kristof, J. Vorholz, J. Liszi, B. Rumpf, G. Maurer, A Simple Effective Pair Potential for the Molecular Simulation of the Thermodynamic Properties of Ammonia, *Mol. Phys.* 97 (1999) 1129
- [15] H. J. C. Berendsen, J. P. M. Postma, W. F. van Gunsteren, J. Hermans, Interaction Models for Water in Relation to Protein Hydration, in *Intermolecular Forces*, Pullmann, B. (Ed.), Reidel, Dordrecht (1981) 331
- [16] H. J. C. Berendsen, J. R. Grigera, T. P. Straatsma, The Missing Term in Effective Pair Potentials, *J. Phys. Chem.*, 79 (1987) 926
- [17] W. L. Jorgensen, J. Chandrasekhar, J. D. Madura, R. W. Impey, M. L. Klein, Comparison of Simple Potential Functions for Simulating Liquid Water, *J. Chem. Phys.* 79 (1983) 926

- [18] K. Watanabe, M. L. Klein, Effective Pair Potentials and the Properties of Water, *Chem. Phys.* 131 (1989) 157
- [19] R. E. Kozack, P. C. Jordan, Polarizability Effects in a Four-Charge Model for Water, *J. Chem. Phys.* 96 (1992) 3120
- [20] M. Medeiros, M. E. Costas, Gibbs Ensemble Monte Carlo Simulation of the Properties of Water with a Fluctuating Charges Model, *J. Chem. Phys.* 107 (1997) 2012
- [21] G. C. Boulougouris, I. G. Economou, D. N. Theodorou, Engineering a Molecular Model for Water Phase Equilibrium over a Wide Temperature Range, *J. Phys. Chem. B* 102 (1998) 1029
- [22] J. R. Errington and A. Z. Panagiotopoulos, A Fixed Point Charge Model for Water Optimized to the Vapor-Liquid Coexistence Properties, *J. Phys. Chem. B*, 102, (1998) 7470
- [23] J. J. de Pablo, J. M. Prausnitz, Phase Equilibria for Fluid Mixtures from Monte Carlo Simulation, *Fluid Phase Eq.* 53 (1989) 177
- [24] J. J. de Pablo, J. M. Prausnitz, H. J. Strauch, P. T. Cummings, Molecular Simulation of Water along the Liquid-Vapor Coexistence Curve from 25 °C to the Critical Point, *J. Chem. Phys.* 93 (1990) 7355
- [25] Y. Guissani, B. Guillot, A Computer Simulation Study of the Liquid-Vapor Coexistence Curve of Water, *J. Chem. Phys.* 98 (1993) 8221
- [26] J. Alexandre, D. J. Tildesley, G. A. Chapela, Molecular Dynamics Simulation of the Orthobaric Densities and Surface Tension of Water, *J. Chem. Phys.* 102 (1995) 4574
- [27] K. Kiyohara, K. E. Gubbins, A. Z. Panagiotopoulos, Phase Coexistence Properties of Polarizable Water Models, *Mol. Phys.* 94 (1998) 803
- [28] M. P. Allen, D. J. Tildesley, *Computer Simulation of Liquids* (Clarendon Press, Oxford, 1987)
- [29] R. F. Cracknell, D. Nicholson, N. G. Parsonage, H. Evans, Rotational Insertion Bias: A Novel Method for Simulating Dense Phases of Structured Particles, with Particular Application to Water, *Mol. Phys.* 5 (1990) 931
- [30] J. I. Siepmann, D. Frenkel, Configurational Bias Monte Carlo: a New Sampling Scheme for Flexible Chains, *Mol. Phys.* 75 (1992) 59
- [31] L. D. J. C. Loyens, B. Smit, K. Esselink, Parallel Gibbs-Ensemble Simulations, *Mol. Phys.* 2 (1995) 171
- [32] B. Smit, Ph. De Smedt, D. Frenkel, Computer Simulations in the Gibbs Ensemble, *Mol. Phys.* 68 (1989) 931
- [33] D. N. Theodorou, U. W. Suter, Geometrical Considerations in Systems with Periodic Boundary Conditions, *J. Chem. Phys.* 82 (1985) 955
- [34] S. W. de Leeuw, J. W. Perram, E. R. Smith, Simulation of Electrostatic Systems in Periodic Boundary Conditions: I. Lattice Sums and Dielectric Constants, *Proc. R. Soc. Lond. A* 373 27 (1980)
- [35] V. I. Harismiadis, J. Vorholz, A. Z. Panagiotopoulos, Efficient Pressure Estimation in Molecular Simulations without Evaluating the Virial, *J. Chem. Phys.* 105 (1996) 8469
- [36] M. Mezei, Theoretical Calculation of the Liquid-Vapor Coexistence Curve of Water, Chloroform and Methanol with the Cavity-Biased Monte Carlo Method in the Gibbs Ensemble, *Mol. Sim.* 9 (1992) 257
- [37] E. Bender, Equations of State Exactly Representing the Phase Behavior of Pure Substances, *Proc. Symp. Thermophys. Prop.* 5 (1970) 227

- [38] M. Mezei, The Effect of the Combined Volume on the Efficiency of Gibbs Ensemble Simulations, *Mol. Sim.* 11 (1993) 395
- [39] J. P. Valleau, Number-dependence Concerns in Gibbs-ensemble Monte Carlo, *J. Chem. Phys.* 108 (1998) 2962
- [40] R. Wiebe, V. L. Gaddy, The Solubility in Water of Carbon Dioxide at 50, 75, and 100°, at Pressures to 700 Atmospheres, *J. Am. Chem. Soc.* 61 (1939) 315
- [41] A. Zawisza, M. Bogusława, Solubility of Carbon Dioxide in Liquid Water and of Water in Gaseous Carbon Dioxide in the Range 0.2 - 5 MPa and at Temperatures up to 473 K, *J. Chem. Eng. Data* 26 (1981) 388
- [42] R. Wiebe, The Binary System Carbon Dioxide - Water under Pressure, *Chem. Rev.* 21 (1941) 475
- [43] C. R. Coan, A. D. King, Jr., Solubility of Water in Compressed Carbon Dioxide, Nitrous Oxide and Ethane. Evidence for Hydration of Carbon Dioxide and Nitrous Oxide in the Gas Phase, *J. Am. Chem. Soc.* 93 (1971) 1857
- [44] Y. D. Zelvenskij, *J. Chem. Ind. (USSR)* 14 (1937) 1250
- [45] K. Tödheide, E. U. Franck, Das Zweiphasengebiet und die kritische Kurve im System Kohlendioxid - Wasser bis zu Drücken von 3500 bar, *Z. Phys. Chem. Neue Folge* 37 (1963) 387
- [46] J. A. Nighswander, N. Kalogerakis, A. K. Mehrotra, Solubilities of Carbon Dioxide in Water and 1 wt % NaCl Solution at Pressures up to 10 MPa and Temperatures from 80 to 200 °C, *J. Chem. Eng. Data* 34 (1989) 355
- [47] B. Rumpf, G. Maurer, An Experimental and Theoretical Investigation on the Solubility of Carbon Dioxide in Aqueous Solutions of Strong Electrolytes, *Ber. Bunsenges. Phys. Chem.*, 97 (1993) 85
- [48] B. Platzer, G. Maurer, Application of a Generalized Bender Equation of State to the Description of Vapour – Liquid Equilibria in Binary Systems, *Fluid Phase Eq.*, 84 (1993) 79

Table 1: Geometry data and potential parameters of the molecular models

	SPC	SPC/E	TIP4P		EPM2
α / deg	109.47	109.47	104.52	$r_{\text{C-O}} / \text{\AA}$	1.149
$r_{\text{O-H}} / \text{\AA}$	1.00	1.00	0.9572	$\sigma_{\text{O}} / \text{\AA}$	3.033
$r_{\text{O-M}} / \text{\AA}$	0.00	0.00	0.15	$\epsilon_{\text{O}}/k / \text{K}$	80.507
$\sigma_{\text{O}} / \text{\AA}$	3.166	3.166	3.154	$\sigma_{\text{C}} / \text{\AA}$	2.757
$\epsilon_{\text{O}}/k / \text{K}$	78.197	78.197	78.020	$\epsilon_{\text{C}}/k / \text{K}$	28.129
q_{O} / e	-0.82	-0.8476	-1.04	q_{O} / e	-0.3256
q_{H} / e	0.41	0.4238	0.52	q_{C} / e	0.6512

Table 2: Literature simulation data taken for testing the code

ES: Ewald Summation, SC: Spherical cutoff, RF: Reaction field

System	Model	Simulation	Treatment of long range electrostatic interactions	Pressure calculation	Ref.
H ₂ O	SPC	NVT-GEMC	ES	-	de Pablo et al. [24]
H ₂ O	SPC	NVT-GEMC cavity bias	SC	-	Mezei [36]
H ₂ O	SPC/E	NVE-MD (EOS)	ES	virial function	Guissani and Guillot [25]
H ₂ O	SPC/E	Slab Geometry MD	ES	virial function	Alejandre et al. [26]
H ₂ O	SPC, SPC/E	NVT-GEMC excluded volume map sampling	ES	virial function	Boulougouris et al. [21]
H ₂ O	TIP4P	NVT-GEMC	SC*	-	de Pablo and Prausnitz [23]
H ₂ O	TIP4P	NVT-GEMC rotational bias	SC	via 2 nd virial coefficient	Cracknell et al. [29]
CO ₂	EPM2	NVT-GEMC	RF	virial function	Harris and Yung [13]

* See de Pablo et al. [24]

Table 3: Simulation results for the binary mixture CO₂-H₂O using the EPM2-model and the SPC-model

T / K	p / MPa	N	ρ^I / (g/cm ³)	ρ^{II} / (g/cm ³)	u^I / (kJ/kg)	u^{II} / (kJ/kg)	x_{CO_2}	y_{CO_2}
348.15	2.500	450	0.944(8)	0.0401(5)	-2140(8)	-11.2(9)	0.0034(13)	0.9777(70)
348.15	2.533	300	0.937(7)	0.0405(7)	-2141(14)	-10.6(2)	0.0039(13)	0.9817(35)
348.15	2.533	600	0.938(5)	0.0407(3)	-2129(11)	-11.1(4)	0.0044(9)	0.9807(32)
348.15	5.000	450	0.939(6)	0.0877(12)	-2121(14)	-23.4(6)	0.0075(14)	0.9889(21)
348.15	5.033	300	0.941(12)	0.0872(22)	-2101(13)	-22.9(5)	0.0106(19)	0.9902(17)
348.15	5.033	300	0.944(8)	0.0878(16)	-2117(21)	-23.0(4)	0.0074(30)	0.9900(17)
348.15	5.033	600	0.935(5)	0.0879(9)	-2113(13)	-23.4(2)	0.0094(23)	0.9907(8)
348.15	7.500	450	0.938(7)	0.1432(24)	-2083(21)	-37.5(7)	0.0144(41)	0.9930(11)
348.15	7.599	300	0.946(7)	0.1457(40)	-2112(27)	-38.1(1.0)	0.0104(49)	0.9917(17)
348.15	7.599	300	0.939(8)	0.1462(24)	-2091(27)	-37.9(1.2)	0.0117(41)	0.9925(30)
348.15	7.599	600	0.942(6)	0.1468(19)	-2112(18)	-39.2(1.5)	0.0094(21)	0.9912(32)
348.15	10.000	450	0.940(7)	0.2172(49)	-2078(27)	-56.3(1.3)	0.0157(52)	0.9940(11)
348.15	10.132	300	0.942(10)	0.2175(61)	-2068(23)	-55.9(1.7)	0.0177(34)	0.9939(21)
348.15	10.132	600	0.945(8)	0.2192(58)	-2088(24)	-56.6(1.7)	0.0138(36)	0.9932(18)
348.15	12.500	450	0.948(10)	0.313(18)	-2091(11)	-78.3(3.9)	0.0140(24)	0.9940(8)
348.15	12.665	300	0.947(10)	0.304(14)	-2103(15)	-75.1(3.3)	0.0113(23)	0.9940(13)
348.15	12.665	600	0.949(8)	0.316(19)	-2091(21)	-79.5(4.2)	0.0145(39)	0.9945(11)

Table 3: Simulation results for the binary mixture CO₂-H₂O using the EPM2-model and the SPC-model (continued)

T / K	p / MPa	N	$\rho^I / (\text{g/cm}^3)$	$\rho^{II} / (\text{g/cm}^3)$	$u^I / (\text{kJ/kg})$	$u^{II} / (\text{kJ/kg})$	x_{CO_2}	y_{CO_2}
373.15	2.500	450	0.913(5)	0.0360(5)	-2061(10)	-10.5(9)	0.0035(6)	0.9459(65)
373.15	2.533	300	0.906(11)	0.0368(5)	-2047(12)	-10.0(4)	0.0049(9)	0.9500(79)
373.15	2.533	600	0.909(12)	0.0367(4)	-2056(18)	-10.6(7)	0.0044(17)	0.9494(56)
373.15	3.700	300	0.912(9)	0.0548(7)	-2050(16)	-14.2(3)	0.0060(13)	0.9679(28)
373.15	3.700	600	0.915(9)	0.0553(6)	-2054(8)	-15.5(9)	0.0049(8)	0.9622(58)
373.15	5.000	450	0.919(5)	0.0775(11)	-2043(3)	-20.5(6)	0.0077(12)	0.9702(33)
373.15	7.500	450	0.917(2)	0.1250(15)	-2030(11)	-32.1(6)	0.0098(19)	0.9801(21)
373.15	7.599	300	0.922(8)	0.1270(26)	-2039(14)	-32.8(1.3)	0.0095(18)	0.9791(40)
373.15	7.599	600	0.922(5)	0.1271(13)	-2045(21)	-33.2(8)	0.0087(22)	0.9776(23)
373.15	10.132	300	0.920(7)	0.1786(43)	-2029(8)	-45.3(1.4)	0.0109(21)	0.9817(41)
373.15	10.132	600	0.925(6)	0.1835(57)	-2019(12)	-46.6(1.3)	0.0130(12)	0.9834(12)
373.15	12.500	450	0.920(11)	0.2427(64)	-2007(27)	-60.1(1.7)	0.0158(45)	0.9860(20)
373.15	15.000	450	0.922(6)	0.3078(92)	-2010(22)	-75.4(1.9)	0.0151(38)	0.9871(16)
373.15	15.198	600	0.925(4)	0.315(13)	-2004(22)	-76.7(2.9)	0.0158(36)	0.9869(24)
373.15	15.198	600	0.921(3)	0.311(11)	-1999(14)	-75.4(3.3)	0.0171(20)	0.9883(8)
373.15	20.265	600	0.926(3)	0.451(14)	-1994(22)	-107(3)	0.0188(39)	0.9879(11)

Table 3: Simulation results for the binary mixture CO₂-H₂O using the EPM2-model and the SPC-model (continued)

T / K	p / MPa	N	$\rho^I / (\text{g/cm}^3)$	$\rho^{II} / (\text{g/cm}^3)$	$u^I / (\text{kJ/kg})$	$u^{II} / (\text{kJ/kg})$	x_{CO_2}	y_{CO_2}
393.15	2.00	300	0.887(8)	0.0259(1)	-1996(10)	-11.7(3.0)	0.0028(9)	0.873(17)
393.15	2.00	600	0.884(7)	0.0257(5)	-1990(8)	-12.0(2.2)	0.0030(5)	0.861(12)
393.15	2.50	450	0.887(9)	0.0333(2)	-1998(13)	-12.0(2.3)	0.0033(10)	0.898(16)
393.15	5.00	300	0.896(9)	0.0706(5)	-1992(16)	-19.5(6)	0.0055(22)	0.9419(66)
393.15	5.00	450	0.892(10)	0.0715(9)	-1983(12)	-19.4(6)	0.0066(15)	0.9470(68)
393.15	5.00	600	0.892(9)	0.0714(9)	-1988(14)	-19.4(3)	0.0064(20)	0.9471(55)
393.15	6.00	300	0.894(12)	0.0868(14)	-1981(10)	-23.0(7)	0.0069(10)	0.9534(51)
393.15	6.00	600	0.885(5)	0.0880(5)	-1961(15)	-24.1(1.2)	0.0096(25)	0.9555(23)
393.15	7.00	300	0.890(13)	0.1033(9)	-1967(18)	-26.6(7)	0.0107(25)	0.9606(66)
393.15	7.00	300	0.885(7)	0.1044(18)	-1954(13)	-26.8(6)	0.0114(16)	0.9625(37)
393.15	7.00	600	0.889(4)	0.1038(15)	-1969(13)	-27.2(1.0)	0.0094(10)	0.9620(51)
393.15	7.50	450	0.894(6)	0.1128(11)	-1974(6)	-30.4(2.5)	0.0091(12)	0.9592(41)
393.15	8.00	300	0.885(5)	0.1211(15)	-1950(17)	-30.9(8)	0.0136(28)	0.9658(26)
393.15	8.00	600	0.893(6)	0.1225(15)	-1967(18)	-31.7(6)	0.0105(22)	0.9641(33)
393.15	10.00	300	0.895(9)	0.1582(40)	-1961(20)	-39.5(1.2)	0.0121(35)	0.9694(38)
393.15	10.00	450	0.896(9)	0.1592(30)	-1963(18)	-40.0(1.1)	0.0126(24)	0.9706(43)
393.15	10.00	600	0.897(8)	0.1592(45)	-1960(21)	-40.6(1.0)	0.0113(35)	0.9669(89)
393.15	12.50	450	0.900(8)	0.2089(66)	-1967(25)	-51.5(1.8)	0.0132(35)	0.9750(34)
393.15	15.00	450	0.905(12)	0.2610(66)	-1957(27)	-63.7(1.9)	0.0142(33)	0.9747(41)

The statistical uncertainties of the results reported in the tables are given in parentheses. For example, the notation 0.887(8) stands for 0.887 ± 0.008 , the notation -19.5(6) stands for $-19.5(6) \pm 0.6$, and the notation -11.7(3.0) means -11.7 ± 3.0 .

Table 4: Simulation results for the binary mixture CO₂-H₂O using the EPM2-model and the TIP4P-model

T / K	p / MPa	N	$\rho^I / (\text{g/cm}^3)$	$\rho^{II} / (\text{g/cm}^3)$	$u^I / (\text{kJ/kg})$	$u^{II} / (\text{kJ/kg})$	x_{CO_2}	y_{CO_2}
393.15	2.00	600	0.916(8)	0.0254(2)	-1976(18)	-11.7(1.3)	0.0020(3)	0.840(12)
393.15	2.50	450	0.909(5)	0.0327(4)	-1967(10)	-12.2(1.4)	0.0031(6)	0.880(13)
393.15	5.00	300	0.912(10)	0.0706(14)	-1959(18)	-20.0(8)	0.0059(15)	0.9327(52)
393.15	5.00	450	0.904(10)	0.0709(12)	-1943(16)	-20.5(2.0)	0.0073(16)	0.9383(88)
393.15	6.00	600	0.914(11)	0.0876(15)	-1953(17)	-24.4(1.1)	0.0065(16)	0.943(11)
393.15	7.50	300	0.913(7)	0.1036(10)	-1945(10)	-27.3(1.1)	0.0080(16)	0.9505(66)
393.15	7.50	450	0.912(4)	0.1118(12)	-1931(11)	-29.7(5)	0.0099(12)	0.9544(33)
393.15	10.00	450	0.921(8)	0.1587(29)	-1945(16)	-41.3(2.2)	0.0099(25)	0.9605(91)
393.15	10.00	600	0.912(5)	0.1580(48)	-1924(22)	-40.3(1.7)	0.0126(25)	0.9652(27)
393.15	12.50	450	0.919(7)	0.2088(33)	-1920(18)	-52.4(1.2)	0.0141(30)	0.9677(33)

c.f. footnote for Table 3

Figure captions

Figure 1: Geometry of the SPC-, SPC/E-, and TIP4P-models for water

Figure 2: Geometry of the EPM2-model for carbon dioxide

Figure 3: VLE of SPC-H₂O:

Comparison of the results of the Bender equation of state (Bender [37]), (solid line) with simulation results

- ▲ Mezei [36]
- ▼ de Pablo et al. [24]
- Boulougouris et al. [21]
- ◇ this work

Figure 4: VLE of SPC/E-H₂O:

Comparison of the results of the Bender equation of state (Bender [37]), (solid line) with simulation results

- ▲ Alejandre et al. [26]
- Boulougouris et al. [21]
- ◇ this work

Figure 5: VLE of TIP4P-H₂O:

Comparison of the results of the Bender equation of state (Bender [37]), (solid line) with simulation results

- ▲ Cracknell et al. [29]
- ▼ de Pablo and Prausnitz [23]
- ◇ this work

Figure 6: Vapor pressure of SPC-, SPC/E, and TIP4P-H₂O:

Comparison of the results of the Bender equation of state (Bender [37]), (solid line) with simulation results. The dashed line shows results calculated from the equation of state for SPC/E-H₂O by Guissani and Guillot [25]

- SPC, Boulougouris et al. [21]
- SPC, this work
- SPC/E, Boulougouris et al. [21]
- SPC/E, this work
- ▲ TIP4P, Cracknell et al. [29]
- △ TIP4P, this work

Figure 7: Heats of vaporization of SPC-, SPC/E-, and TIP4P-H₂O:

Comparison of the results of the Bender equation of state (Bender [37]), (solid line) with simulation results

- SPC
- SPC/E
- △ TIP4P

Figure 8: SPC-, SPC/E, and TIP4P-H₂O:p- δ h-diagram

Comparison of the results of the Bender equation of state (Bender [37]), (solid line) with simulation results

- SPC
- SPC/E
- ▲ TIP4P

Figure 9: VLE of EPM2-CO₂: T- ρ -diagram

Comparison of the results of the Bender equation of state (Bender [37]), (solid line) with simulation results

- ▲ Harris and Yung [13]
- ◇ this work

Figure 10: Vapor pressure of EPM2-CO₂:

Comparison of the results of the Bender equation of state (Bender [37]), (solid line) with simulation results

- ▲ Harris and Yung [13]
- ◇ this work

Figure 11: Heat of vaporization of EPM2-CO₂:

Comparison of the results of the Bender equation of state (Bender [37]), (solid line) with simulation results

- ▲ Harris and Yung [13]
- ◇ this work

Figure 12: EPM2-CO₂: p- ρ -diagram

Comparison of the results of the Bender equation of state (Bender [37]), (solid line) with simulation results of this work (open symbols)

Figure 13: EPM2-CO₂: p- δ h-diagram

Comparison of the results of the Bender equation of state (Bender [37]), (solid line) with simulation results of this work (open symbols)

Figure 14: SPC-H₂O - EPM2-CO₂: p-x-y-diagram at T = 348.15 K

Simulation results of this work for the equilibrium concentrations are compared with experimental data and a thermodynamic model:

- ▲ Wiebe and Gaddy [40]
- Zawisza and Boguslawka [41]
- ▼ Wiebe [42]
- Coan and King [43]
- ◇ this work
- thermodynamic model, Rumpf and Maurer [47]

Figure 15: SPC-H₂O - EPM2-CO₂: p-x-y-diagram at T = 373.15 K

Simulation results of this work for the equilibrium concentrations are compared with experimental data and a thermodynamic model:

- ▲ Wiebe and Gaddy [40]
- ▶ Zelvenskij [44]
- ◀ Tödheide and Franck [45]
- Coan and King [43]
- ◇ this work
- thermodynamic model, Rumpf and Maurer [47]

Figure 16: SPC-H₂O - EPM2-CO₂: p-x-y-diagram at T = 393.15 K

Simulation results of this work for the equilibrium concentrations are compared with experimental data and a thermodynamic model:

- ◆ Nighswander et al. [46]
- ◇ this work
- thermodynamic model, Rumpf and Maurer [47]

Figure 17: SPC-H₂O - EPM2-CO₂: p-ρ-diagram at T = 393.15 K

Simulation results of this work (◇) for the densities of the coexisting phases. The vapor phase data are compared with results for pure carbon dioxide (dashed line) from the Bender equation of state (Bender [37]). The liquid densities are compared with experimental results (●) for the densities of the binary system by Nighswander et al. [46] and results of the Bender equation of state for the densities of the pure components (solid lines). Also, predictions of a generalized Bender equation of state for the binary system (Platzer and Maurer [48]) are shown (dashed lines).

Figure 18: TIP4P-H₂O - EPM2-CO₂: p-x-y-diagram at T = 393.15 K

Simulation results of this work for the equilibrium concentrations are compared with experimental data and a thermodynamic model:

- ◆ Nighswander et al. [46]
- ◇ this work
- thermodynamic model, Rumpf and Maurer [47]

Figure 19: TIP4P-H₂O - EPM2-CO₂: p-ρ-diagram at T = 393.15 K

Simulation results of this work (◇) for the densities of the coexisting phases are compared with results of the Bender equation of state (Bender [37]) for the densities of the pure components (solid lines) and with predictions of a generalized Bender equation of state (Platzer and Maurer [48]) for the binary system (dashed lines)

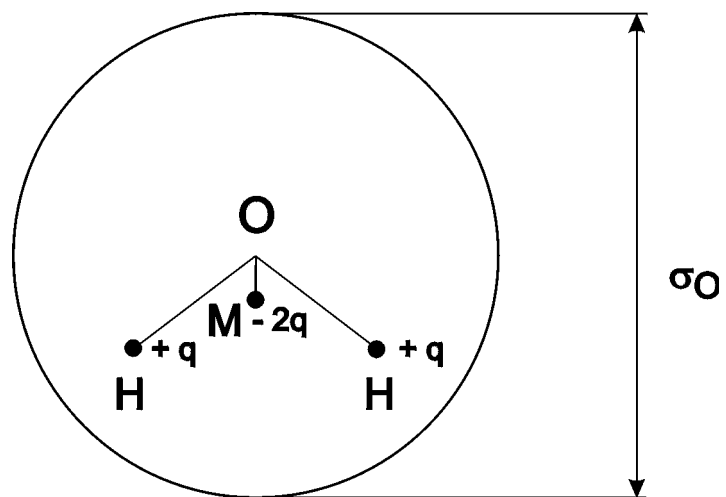


Figure 1
(Vorholz et al.)

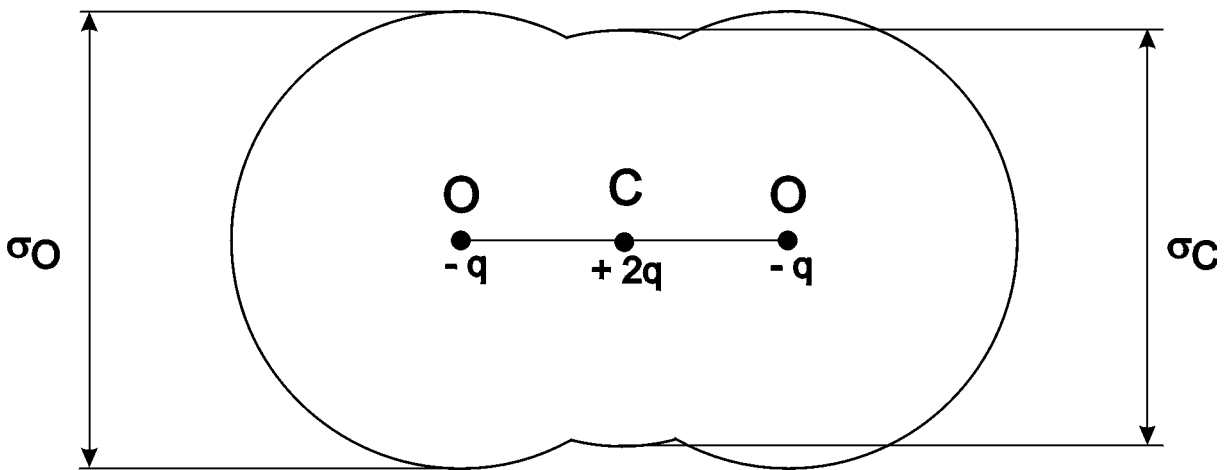


Figure 2
(Vorholz et al.)

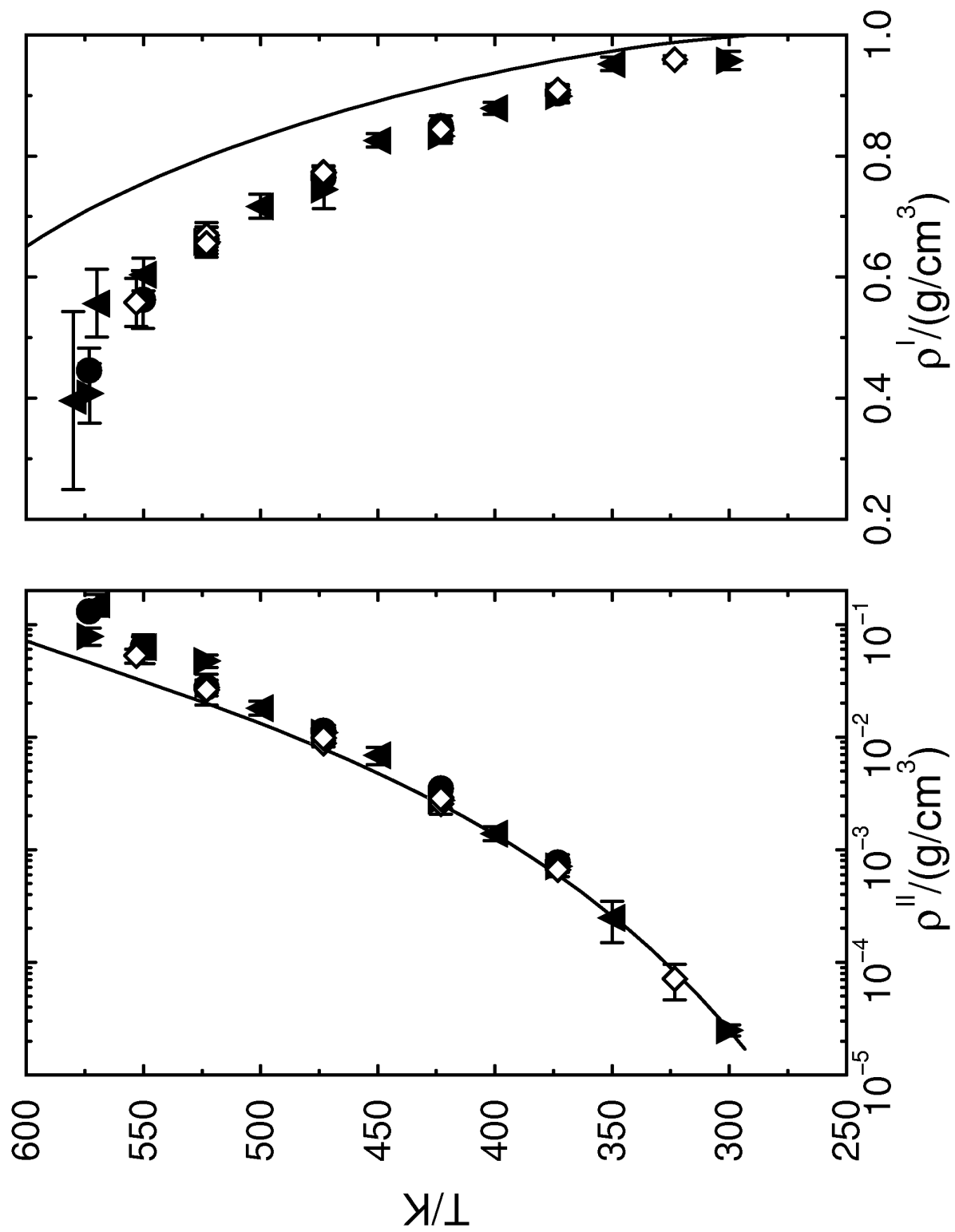


Figure 3
(Vorholz et al.)

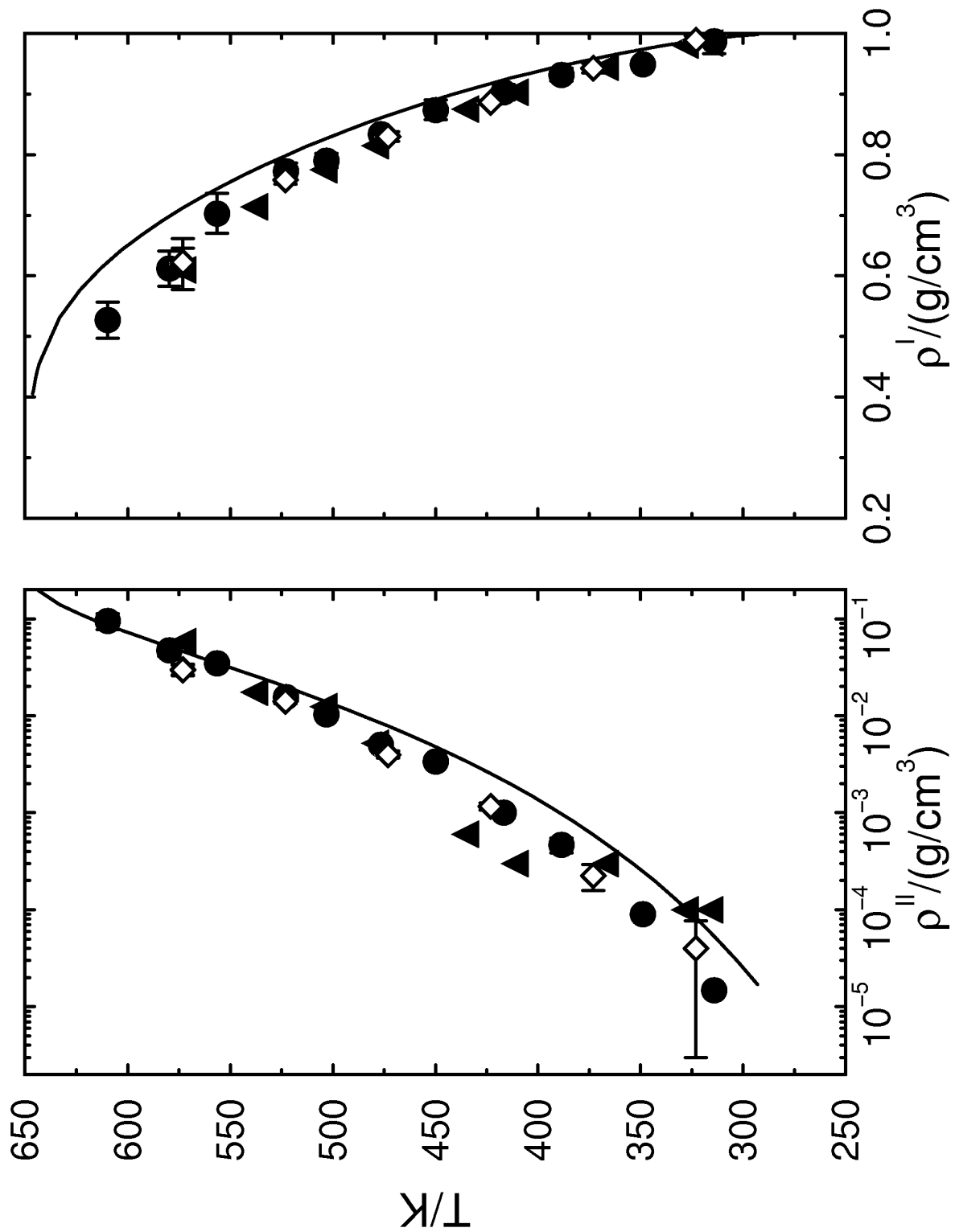


Figure 4
(Vorholz et al.)

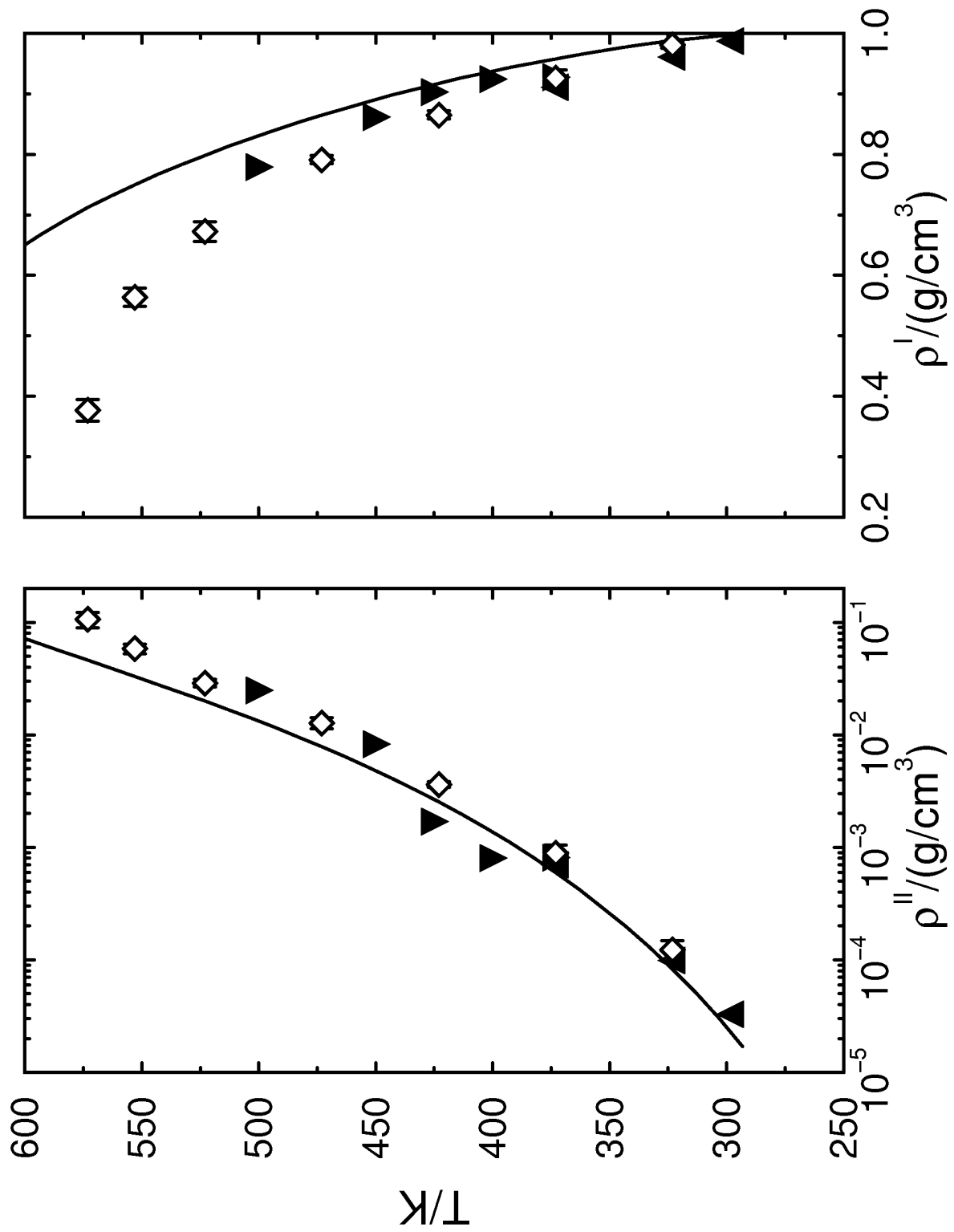


Figure 5
(Vorholz et al.)

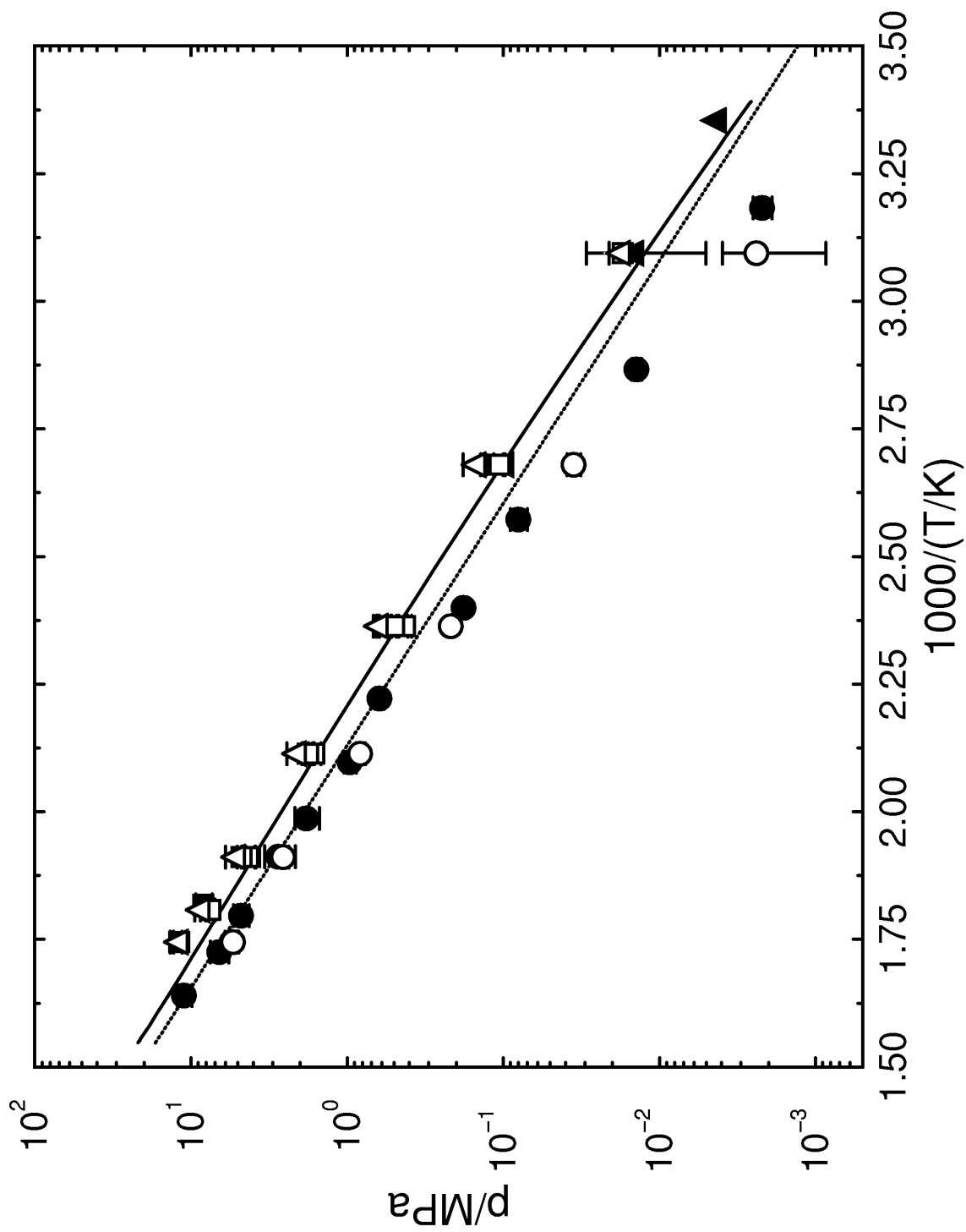


Figure 6
(Vorholz et al.)

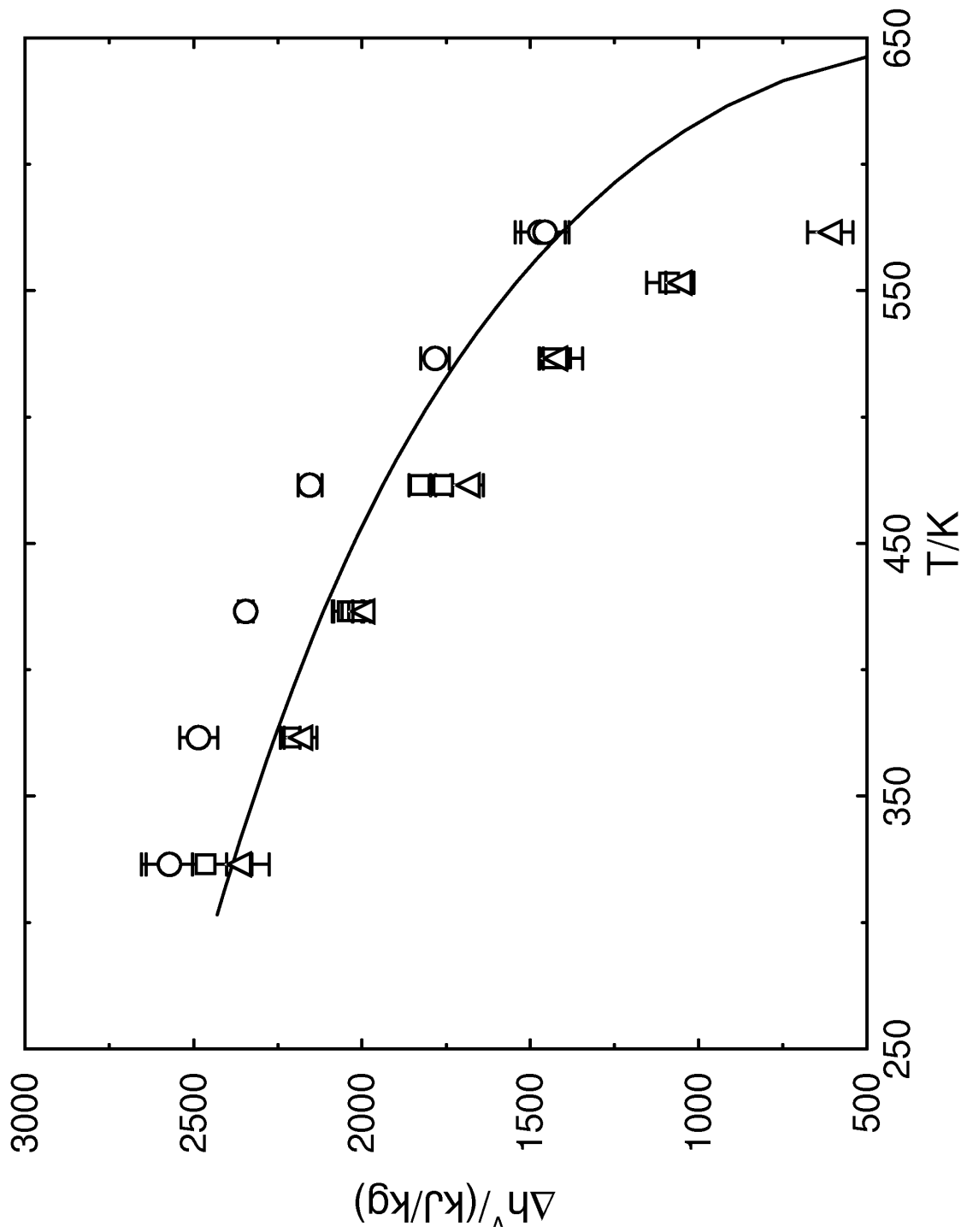


Figure 7
(Vorholz et al.)

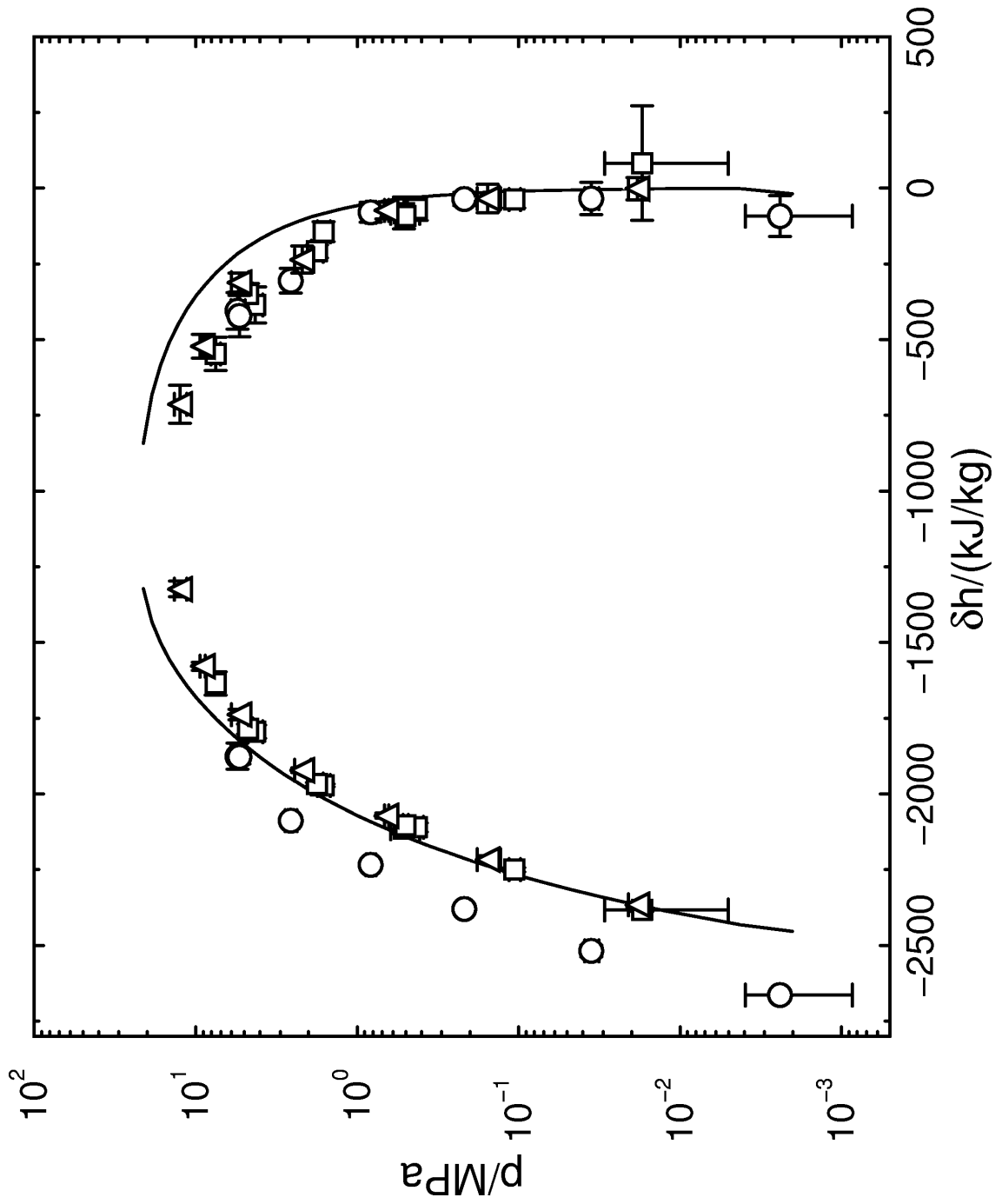


Figure 8
(Vorholz et al.)

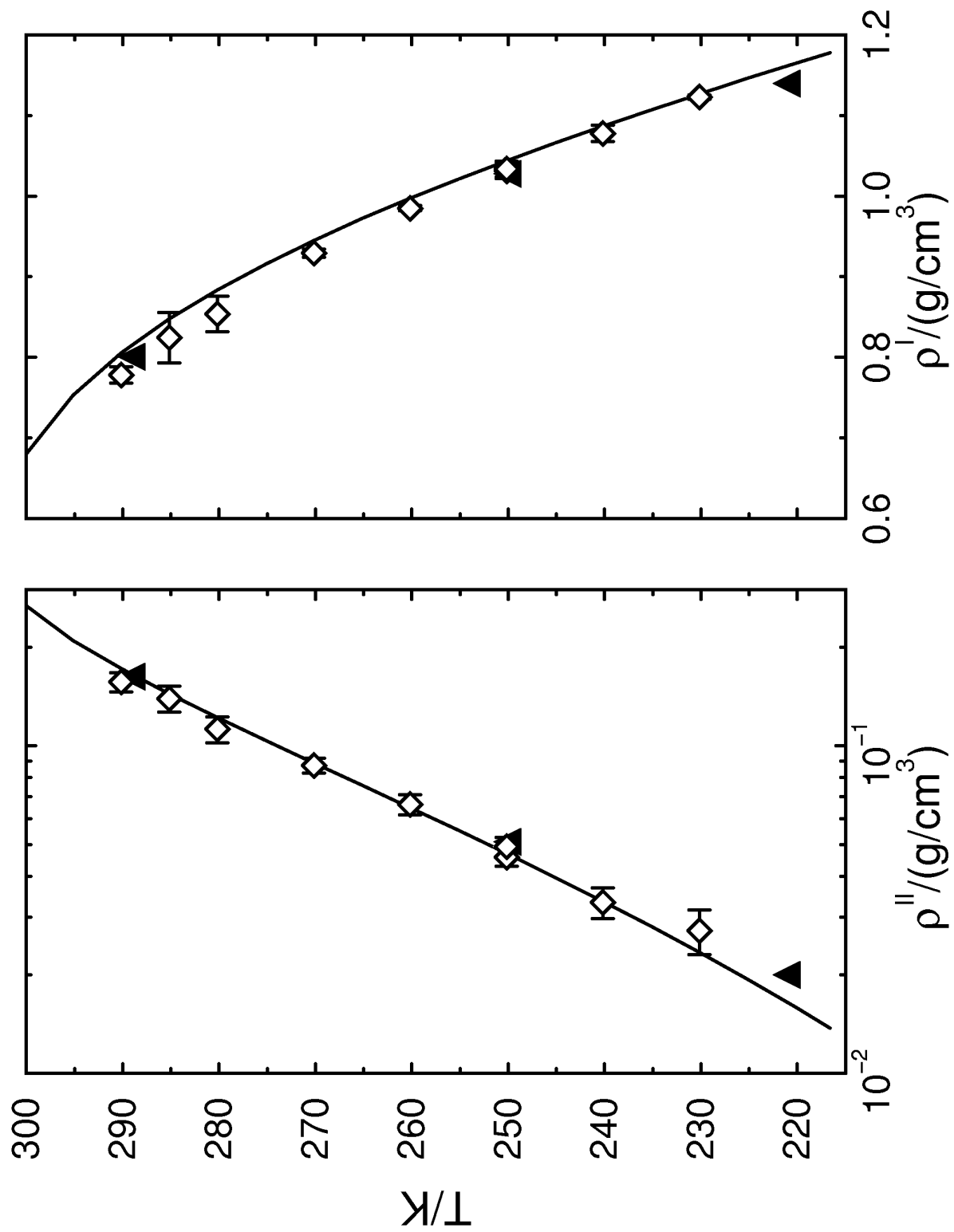


Figure 9
(Vorholz et al.)

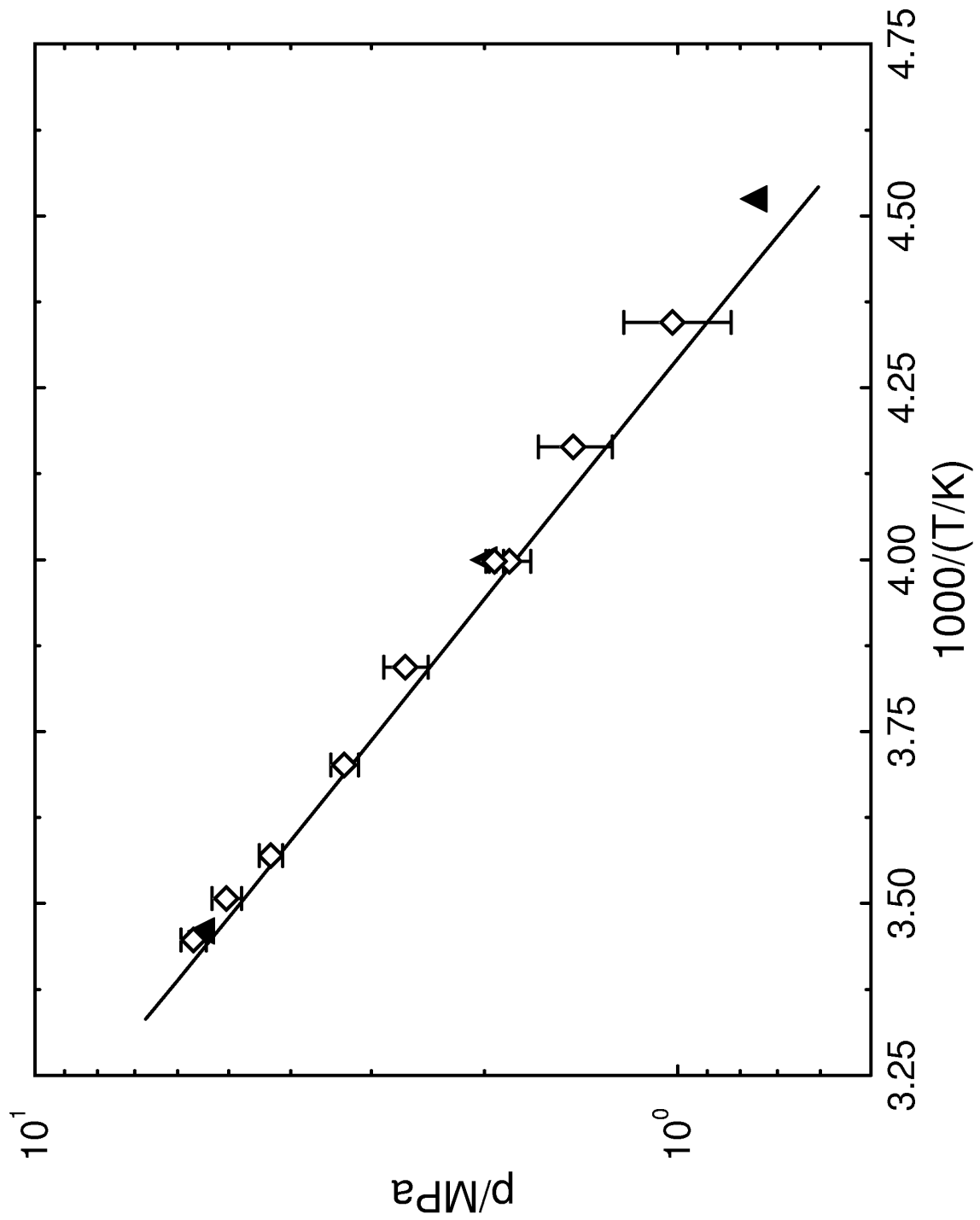


Figure 10
(Vorholz et al.)

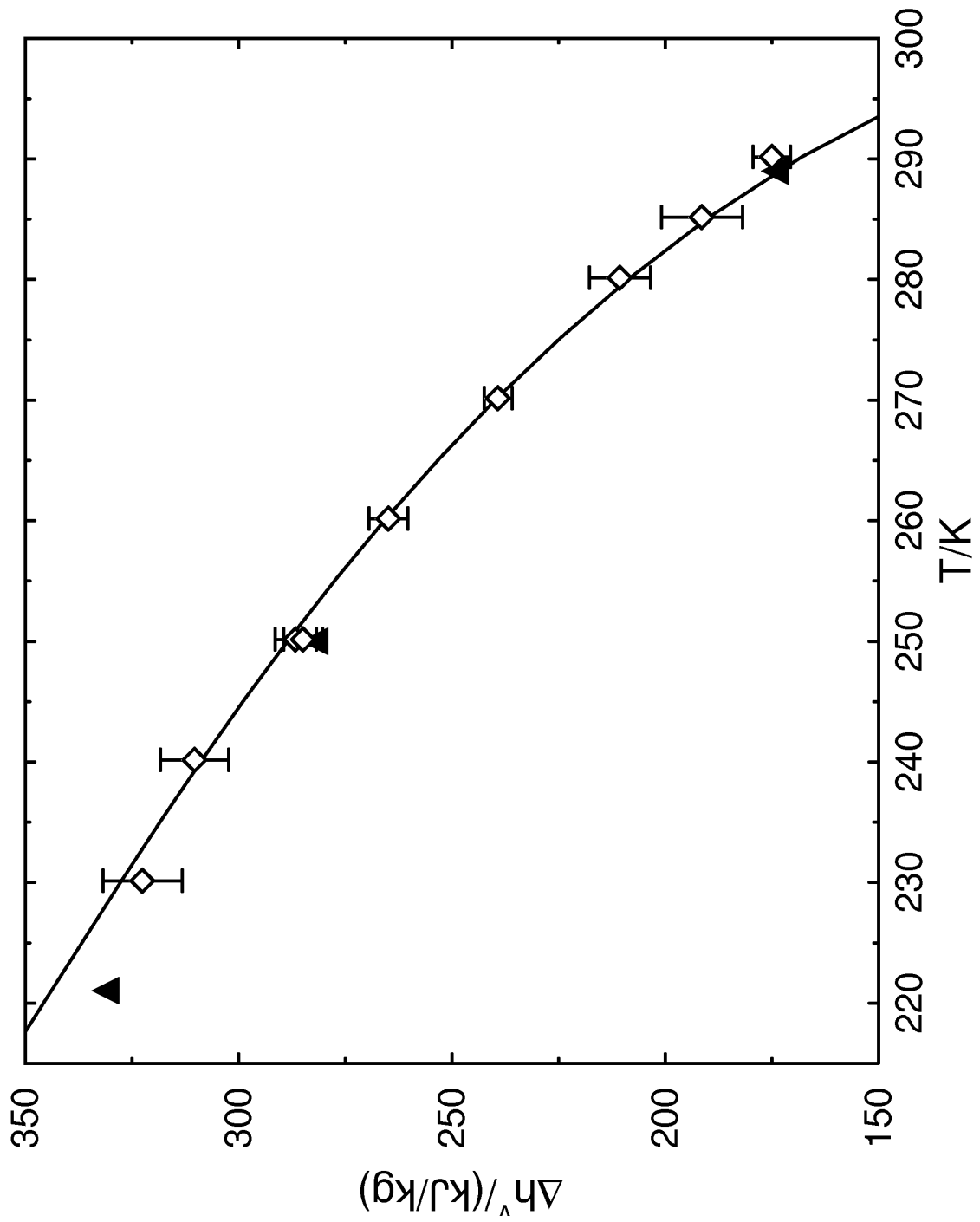


Figure 11
(Vorholz et al.)

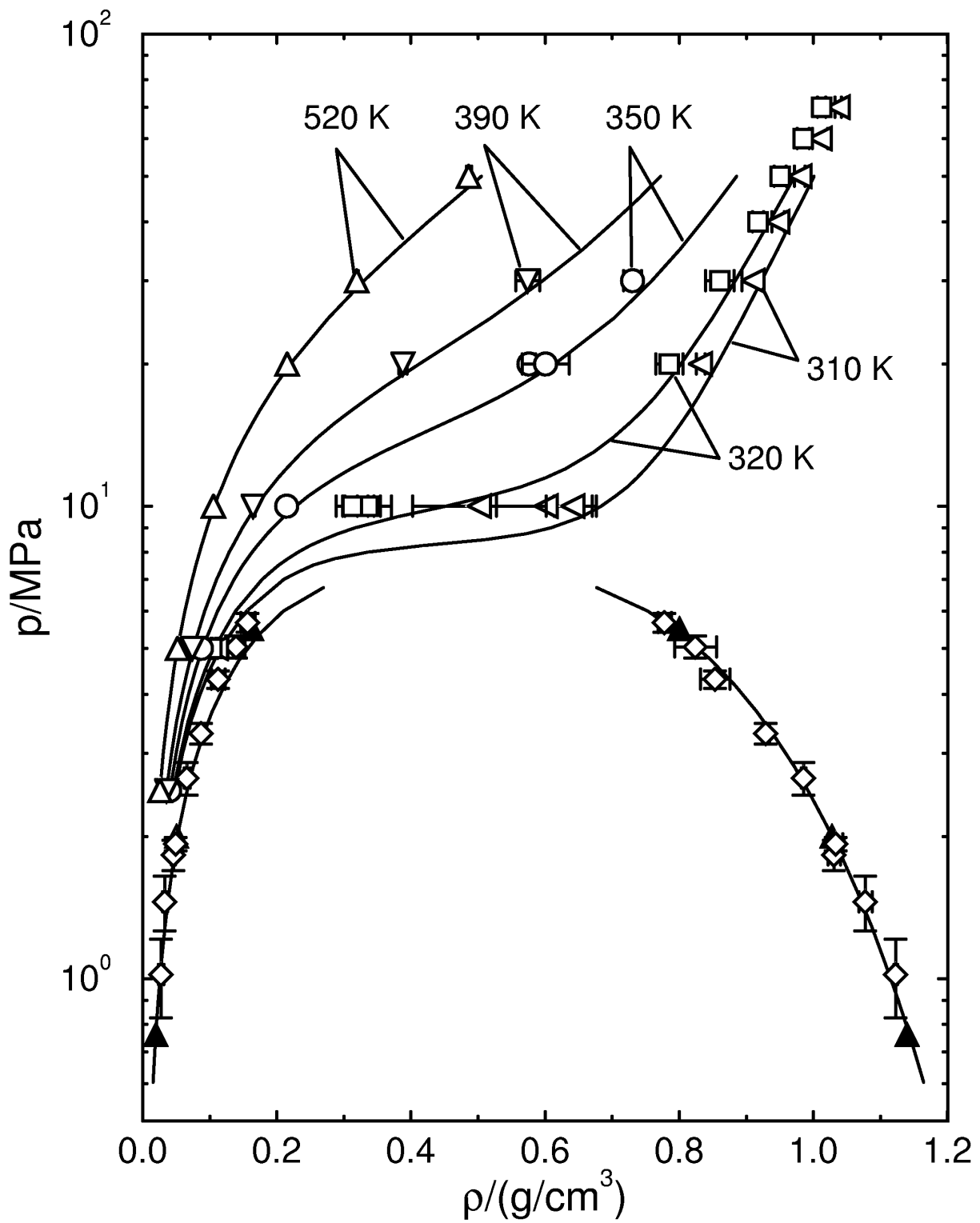


Figure 12
(Vorholz et al.)

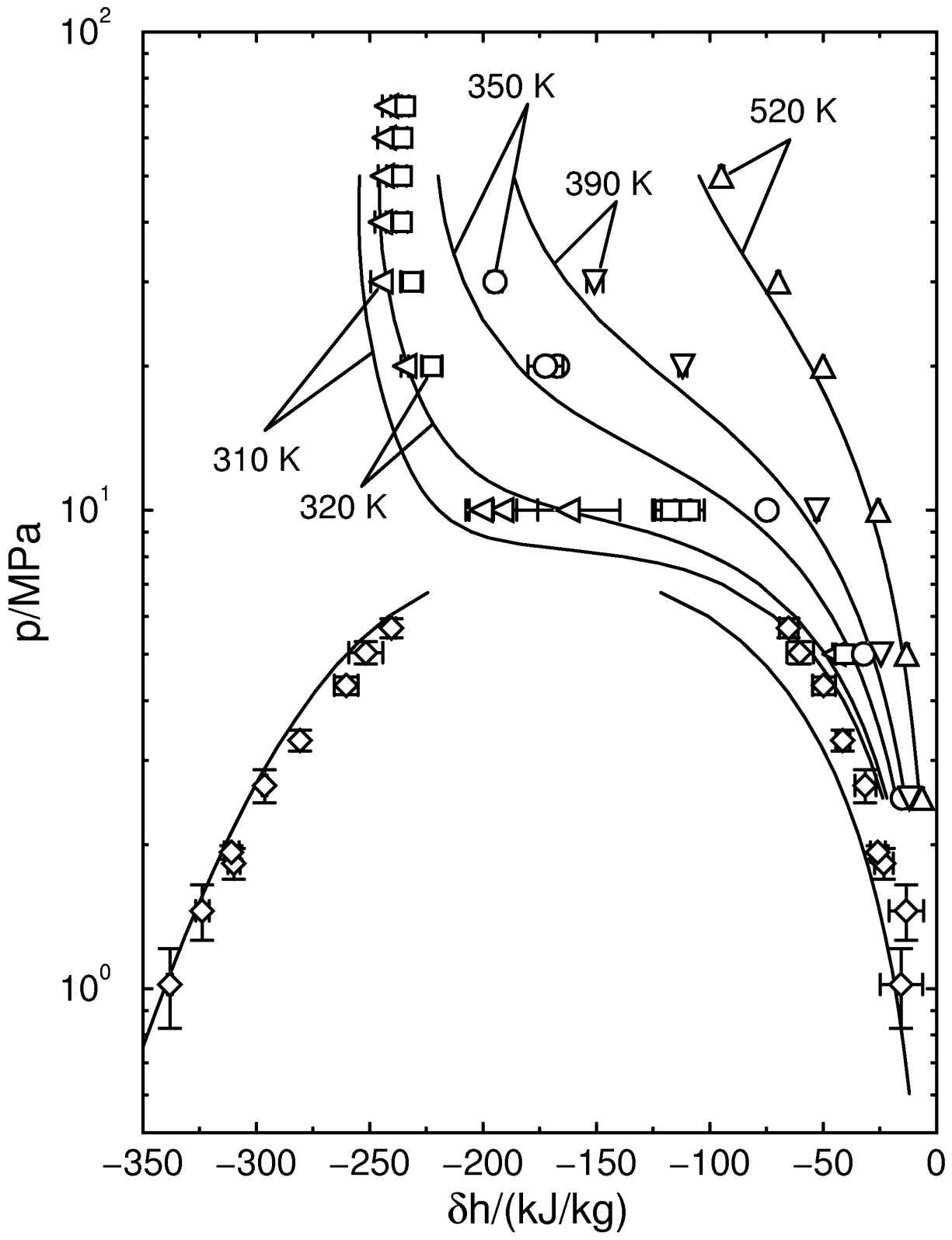


Figure 13
 (Vorholz et al.)

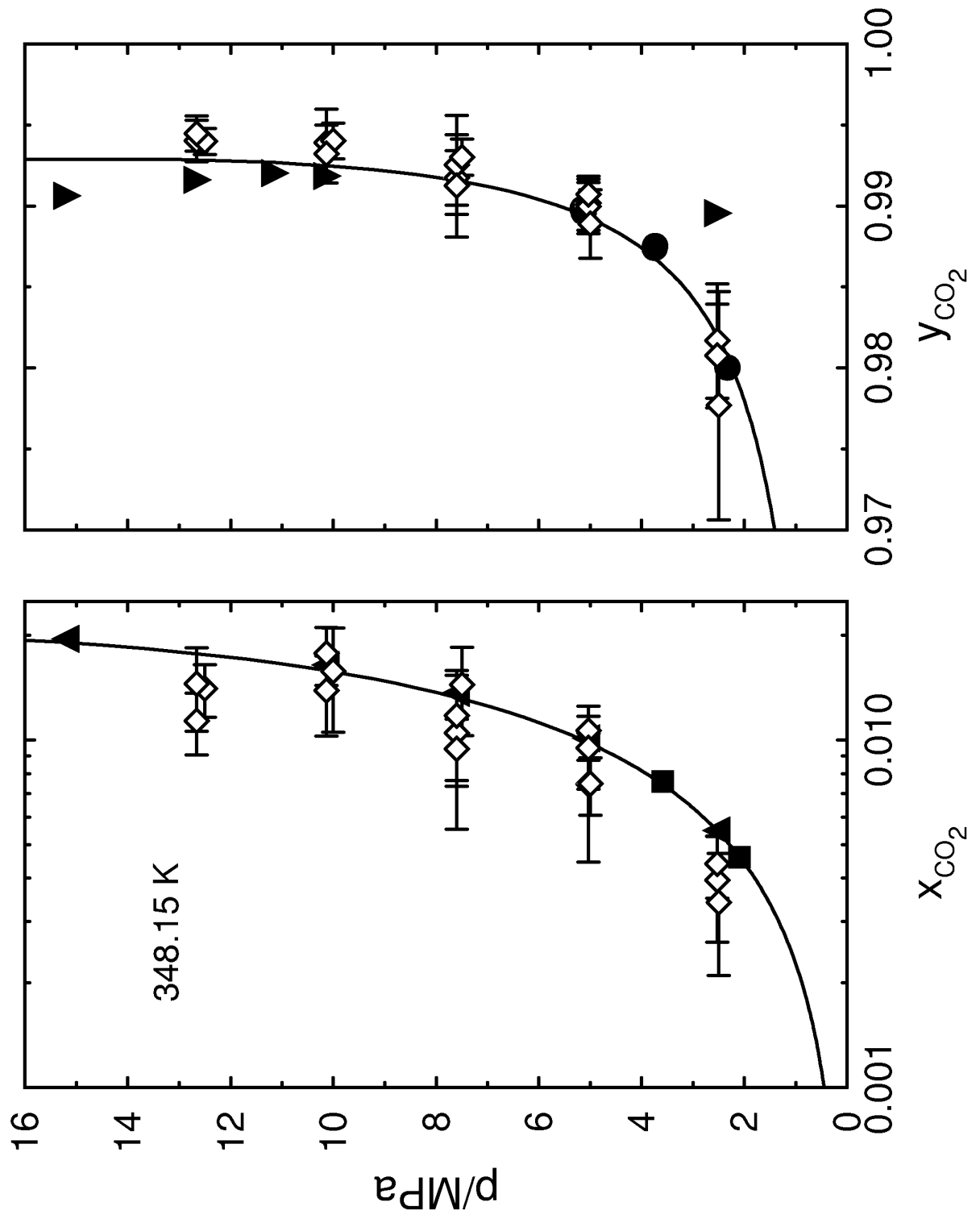


Figure 14
(Vorholz et al.)

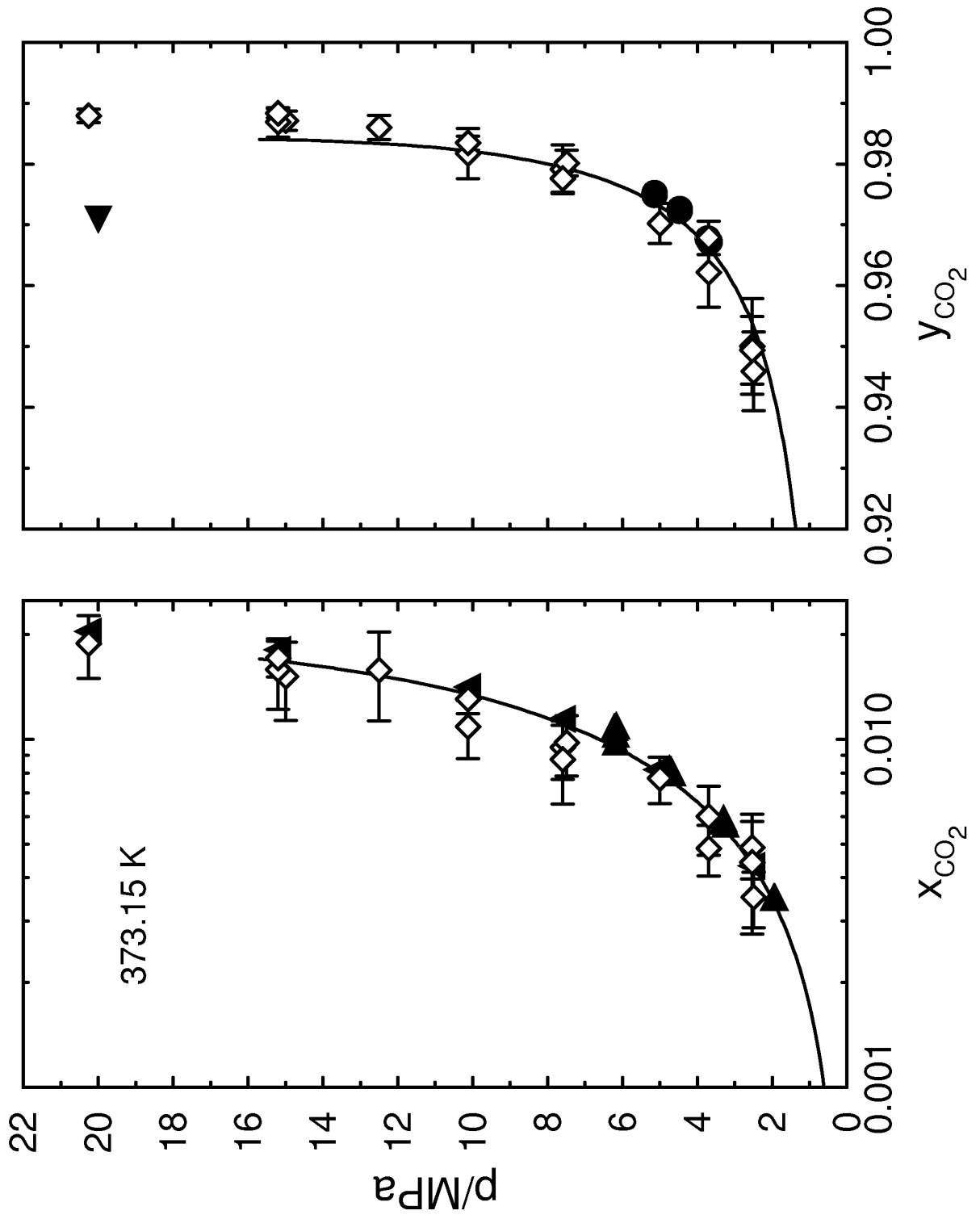


Figure 15
(Vorholz et al.)

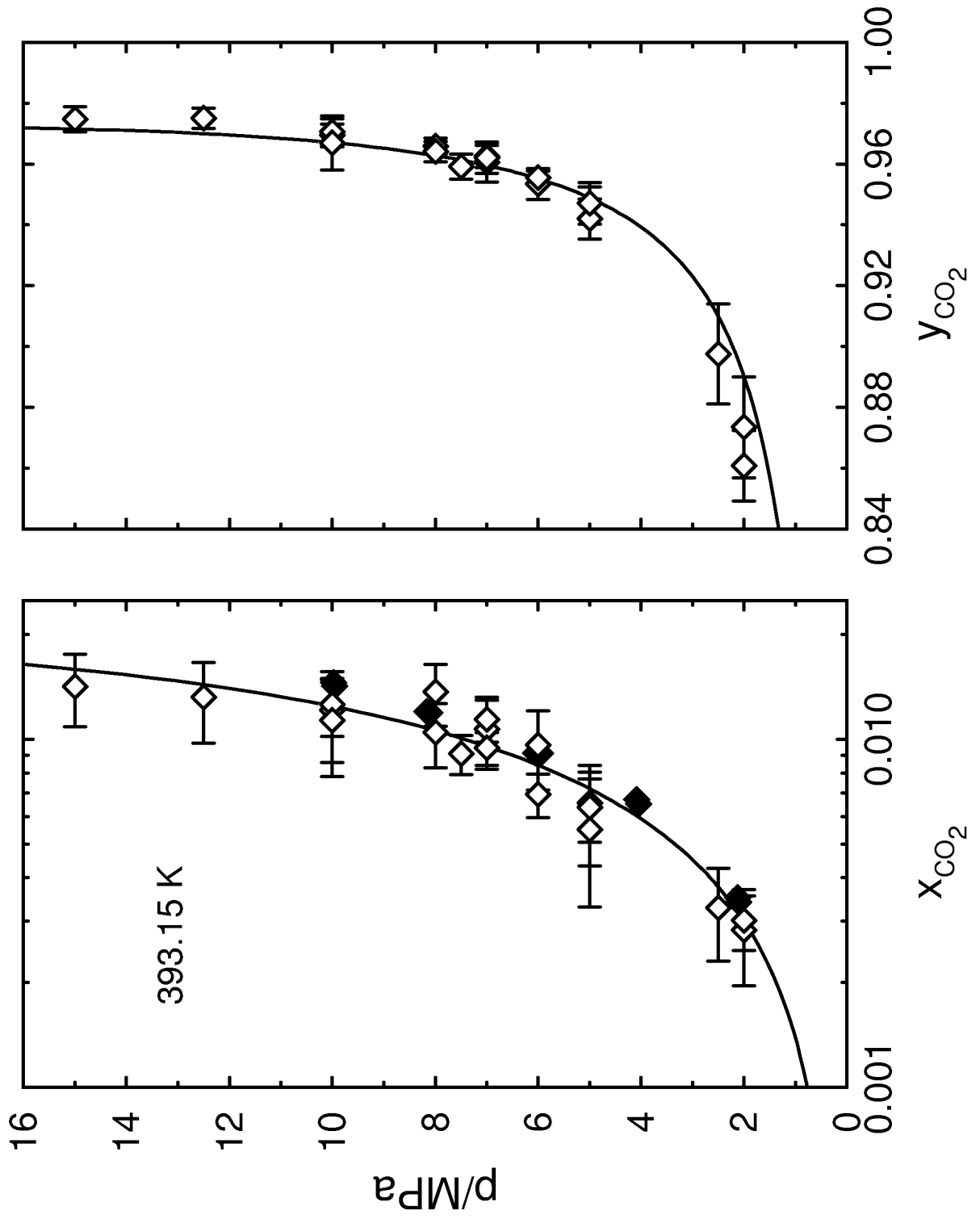


Figure 16
(Vorholz et al.)

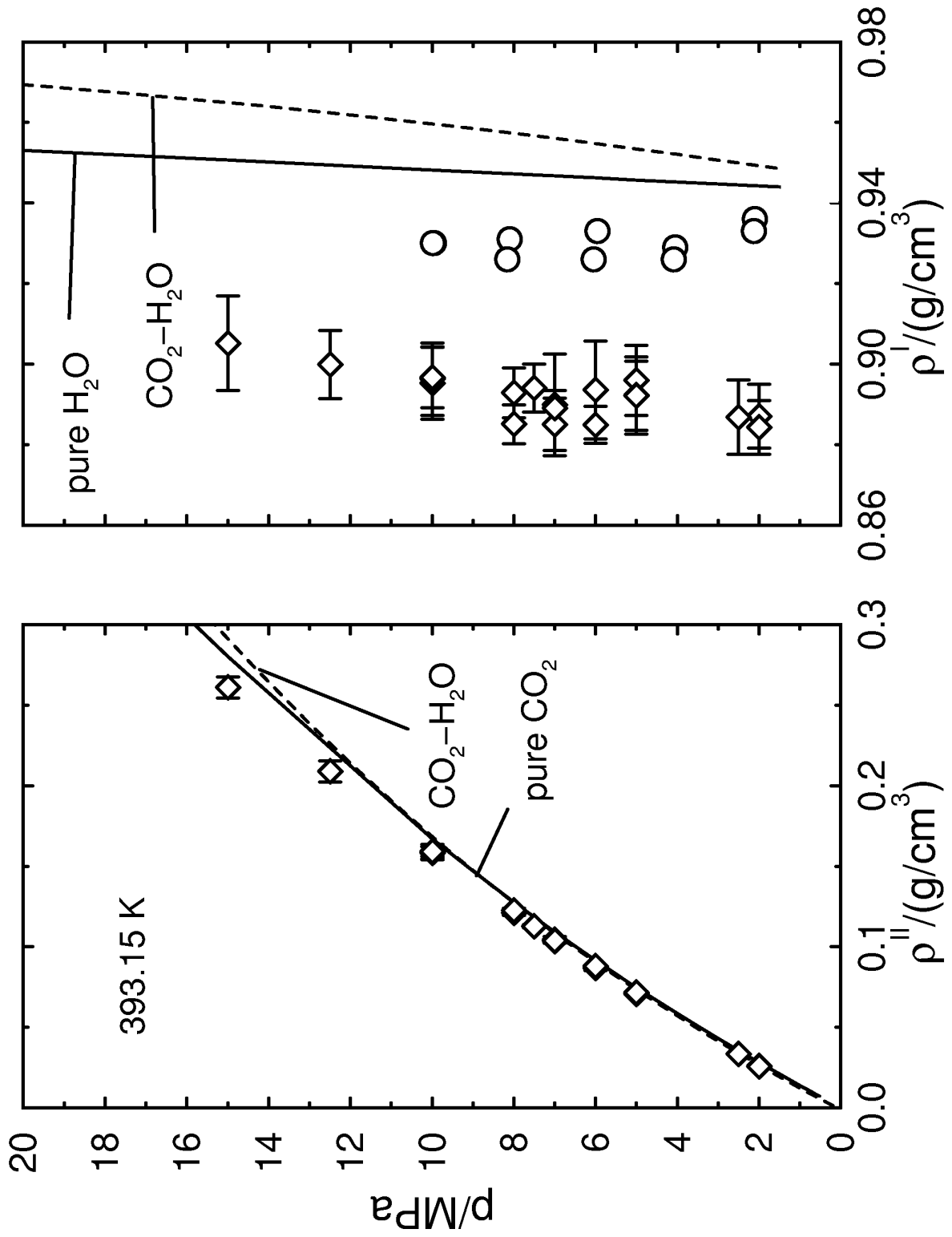


Figure 17
(Vorholz et al.)

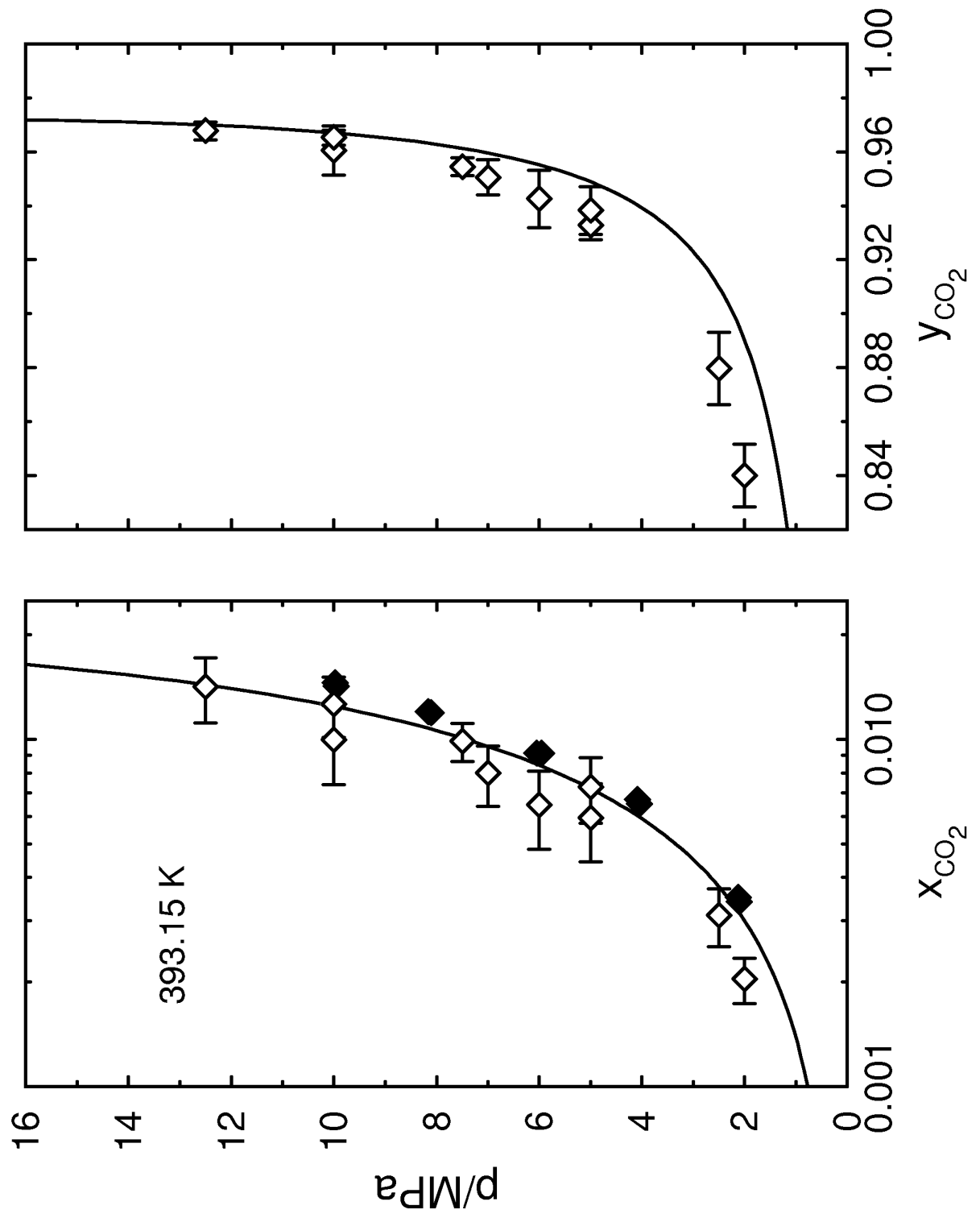


Figure 18
(Vorholz et al.)

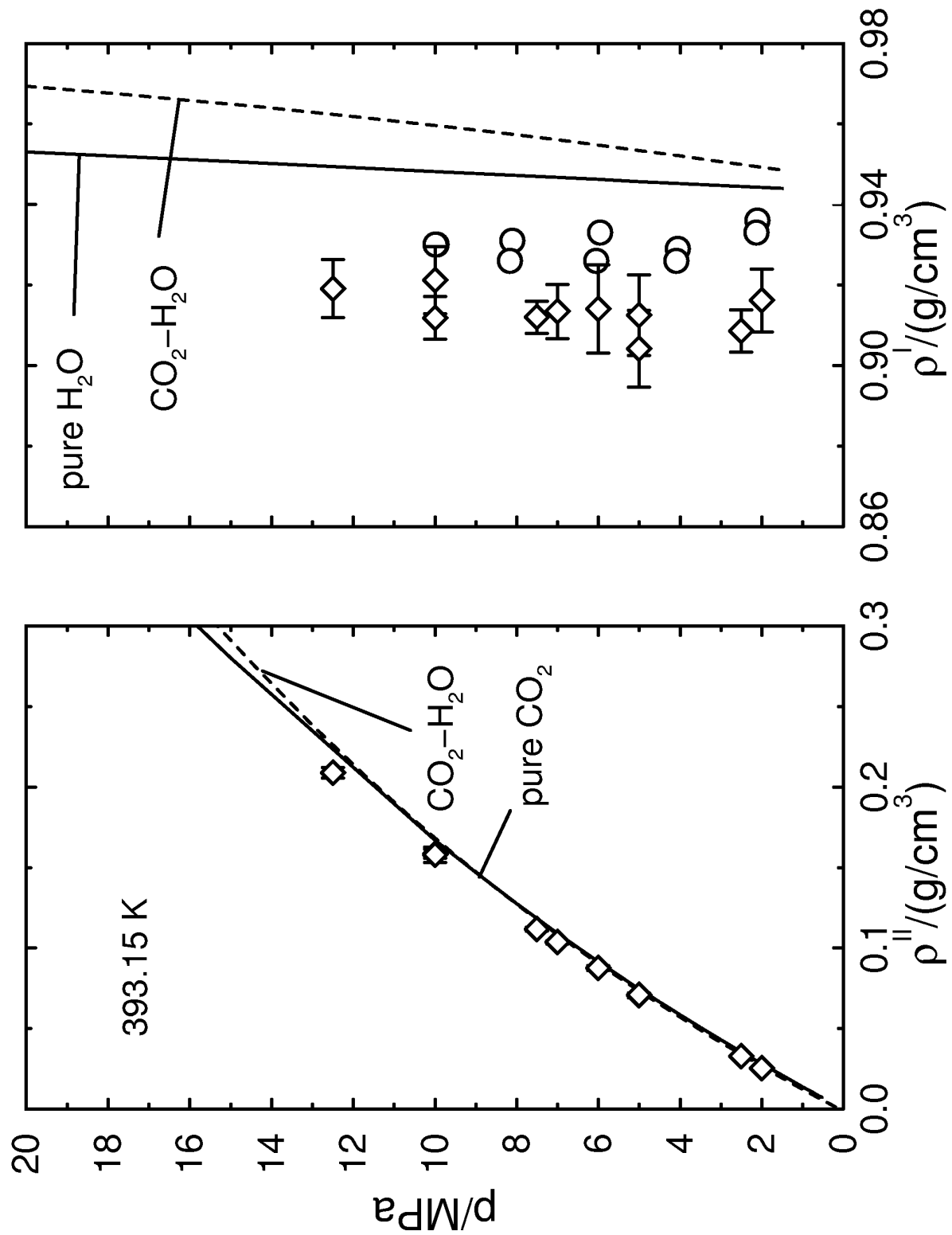


Figure 19
(Vorholz et al.)